Applied Catalysis B: Environmental 96 (2010) 245–266

Contents lists available at ScienceDirect

Applied Catalysis B: Environmental

journal homepage: www.elsevier.com/locate/apcatb

Review

Tungsten-based materials for fuel cell applications

Ermete Antolini[a,b,*], Ernesto R. Gonzalez[b]

[a] Scuola di Scienza dei Materiali, Via 25 aprile 22, 16016 Cogoleto, Genova, Italy
[b] Instituto de Química de São Carlos, USP, C.P. 780, São Carlos, SP 13560-970, Brazil

ARTICLE INFO

Article history:
Received 5 December 2009
Received in revised form 19 February 2010
Accepted 25 February 2010
Available online 6 March 2010

Keywords:
Tungsten
Fuel cells
Catalysts
Nanomaterials

ABSTRACT

Tungsten-based materials can play different roles in fuel cell systems. They are the only compounds which can be used as catalysts, co-catalysts, catalyst supports and electrolytes in different types of fuels cells. In particular, tungsten-based materials fulfill the requirements for their use as thermally stable carbon-alternative catalyst supports and Nafion®-alternative proton conducting electrolytes in fuel cells operating at intermediate temperature. In this work an overview of the use of tungsten-containing materials in fuel cells is presented.

Contents

1. Introduction 246
2. Tungsten-based materials as anode and cathode catalysts for low-temperature fuel cells 246
   2.1. Tungsten bronzes 246
   2.2. Tungsten carbides 246
      2.2.1. Tungsten carbides as anode and cathode catalysts for PEMFCs 247
      2.2.2. Tungsten carbide as anode catalyst for DMFCs 248
      2.2.3. Tungsten carbide as anode catalyst for MFCs 249
   2.3. Tungsten nitrides 249
3. Tungsten-based materials as anode and cathode co-catalysts 250
   3.1. WO_x as co-catalyst in Pt-WO_x 250
      3.1.1. Early studies on Pt-WO_x as catalyst for hydrogen and methanol oxidation 250
      3.1.2. Recent studies on Pt-WO_x and Pt-Ru-WO_x catalysts for H_2/CO and CH_3OH oxidation 250
   3.2. Metal-tungsten carbide composite catalysts 251
   3.3. M-W (M = Pt, Pd) and M-Ru-W (M = Pt, Se) catalysts (with alloyed and non-alloyed W(0)) 253
   3.4. Pt-polyoxometallates and Pt-heteropolyacids 255
   3.5. K_2WO_4 in MCFCs 256
4. Tungsten oxides and carbides as carbon-alternative catalyst supports 256
   4.1. WO_3 256
   4.2. WC and W_2C 257
5. Tungsten-based proton conducting materials in composite membranes 259
   5.1. Heteropolyacids (HPAs) 259
      5.1.1. Early studies at CNR-ITAE, Messina, Italy 260
      5.1.2. Tungsten-based HPAs in inorganic–organic membranes for use at temperatures >100 °C 260
      5.1.3. Anhydrous PWA-containing proton-conducting membranes 262
   5.2. $WO_3 \cdot 2H_2O$ 263
6. Conclusions 264
   Acknowledgment 264
   References 264

* Corresponding author at: Instituto de Química de São Carlos, USP, C.P. 780, São Carlos, SP 13560-970, Brazil. Tel.: +55 33739899; fax: +55 33739895.
E-mail address: ermantol@libero.it (E. Antolini).

0926-3373/$ – see front matter © 2010 Elsevier B.V. All rights reserved.
doi:10.1016/j.apcatb.2010.02.039

1. Introduction

Tungsten is an element of the third transition series of the periodic table. Of all metals in pure form, tungsten has the highest melting point (3.422 °C), the lowest vapor pressure, the lowest coefficient of thermal expansion and, at temperatures above 1.650 °C, the highest tensile strength. The most common oxidation state of tungsten is +6, but it exhibits all oxidation states from −1 to +6 [1]. Tungsten typically combines with oxygen to form stoichiometric tungsten trioxide, WO_3, and lower non-stioichiometric oxides, WO_x, where $2 < x < 3$. Apart WO_3, only three stable tungsten oxides exist: β-oxide ($W_{20}O_{58}$), γ-oxide ($W_{18}O_{49}$), and δ-oxide (WO_2) [2]. All other compounds are either metastable or consist of mixtures and solid solutions of these three phases and WO_3. WO_3 is an *n*-type semiconductor with a reported bandgap of about 2.6 to 2.8 eV [3]. The intrinsic electric conductivity in tungsten oxide arises from its nonstoichiometric composition, giving rise to a donor level formed by oxygen-vacancy defects in the lattice [3], with electrical resistivity decreasing from about 1 ohm cm for WO_2 to a minimum of 0.1 ohm cm for $WO_{2.75}$, then rising sharply to 2×10^5 ohm cm as the composition tends to WO_3. All tungsten oxides are insoluble both in cold and hot water [4]. WO_3 is insoluble in acid as well [5], whereas WO_2 is soluble in acid and alkaline solution. In aqueous alkaline solutions WO_3 forms tungstate ions, WO_4^{2-}. Aqueous tungstate solutions are noted for the formation of heteropoly acids and polyoxometallate anions under neutral and acidic conditions.

Tungsten carbides (W_2C and WC) are some of the hardest carbides, with a melting point of 2770 °C for WC and 2780 °C for W_2C. WC is an efficient electrical conductor, but W_2C is less so. There are two forms of WC, a hexagonal form, α-WC, and a cubic high temperature form, β-WC, which has the rock salt structure [6]. WC belongs to a group of materials, in which elements like carbon (or nitrogen, silicon or phosphor) atoms occupy the interstitial lattice positions of the metal. These materials show remarkable catalytic activities, which have been attributed to a distinct electronic structure induced by the presence of carbon, nitrogen or phosphorous in the metal lattice. In the case of tungsten carbide, its catalytic activity has been explained by the filling of the d-states at the Fermi level of tungsten by the alloying carbon [7]. Tungsten carbide behaves similarly to unalloyed tungsten and is resistant to chemical attack, however, when exposed to air, surface oxidation takes place and advances with time [8]. When exposed to water, tungsten carbide undergoes continuous oxidation and dissolution. This process is pH dependent and follows zero-order kinetics [9]. The surface oxidation of tungsten carbide preferentially progresses on sites, where oxide species already exist [10]. It leads to a simultaneous oxidation of tungsten and carbon.

Tungsten-containing materials can play different roles in fuel cells, as catalysts, co-catalysts, catalyst supports and proton conducting materials in membranes. These materials have been tested for the use in various types of fuel cells, as polymer electrolyte membrane fuel cells fuelled with hydrogen (PEMFCs), methanol (DMFCs) or ethanol (DEFCs), microbial fuel cells (MFCs) and molten carbonate fuel cells (MCFCs). In this work an overview of the use of tungsten-containing materials in fuel cells is presented.

2. Tungsten-based materials as anode and cathode catalysts for low-temperature fuel cells

2.1. Tungsten bronzes

The tungsten bronzes, M_xWO_3, where M is any one of several metals, and $0 < x < 1$, possess all the characteristics of a potential electrocatalyst for acidic fuel cells. They are acid stable, electrically conductive, and can exist with a variation in oxygen stoichiometry, indicating that they can gain and lose oxygen readily. In the decades 1960s and 1970s, research focused on M_xWO_3 for their possible use as electrode materials for the oxygen reaction reduction (ORR) and hydrogen oxidation reaction (HOR) in fuel cells, and the results were conflicting. Sodium tungsten bronze, Na_xWO_3, is a nonstoichiometric compound with *x* a continuous variable from 0 to 1. The compound comprises a WO_3 matrix containing interstitial sodium ions and an equivalent number of quasi-free electrons [11]. When $x > 0.25$, the electrons occupy a conduction band and bestow metallic conductivity on the compound. Na_xWO_3 possess a high resistance to chemical attack by strong acids. Sepa et al. [12] prepared electrodes from $Na_{0.6}WO_3$ crystals. In oxygen-saturated H_2SO_4 solutions, the electrodes were stable even at high potentials, and were more active for the ORR than platinum electrodes. A subsequent work, however, demonstrated that the high catalytic activity required the presence of about 100 ppm platinum in the crystals [13]. McHardy and Bockris [14] observed that when a metallic crystal of Na_xWO_3 was used as an oxygen electrode in acidic solution, sodium was lost from the crystal by anodic dissolution, leaving a thin semiconducting layer on the surface. The composition change in the surface layer corresponded to a decrease in *x* from ~0.7 to ~0.25 for a crystal free of impurities, and from ~0.7 to ~0.05 for a crystal containing traces of platinum. The difference may result from more rapid hole injection in the latter case, associated with the enhanced rate of oxygen reduction. Broyde [15] found that rare earth tungsten bronzes and several transition metal-tungsten mixed oxides catalyze the electrochemical oxidation of hydrogen in acid media. The electrochemical reduction of oxygen in acid solutions was catalyzed not only by these materials, but by all the tungsten-oxygen systems that are acid stable and electrically conductive, whether or not a metal atom is inserted into their structure. Thus $WO_{2.72}$, $WO_{2.9}$ and M_xWO_3 (M = Na, K, Ba, Pb, Tl, U, Cd) served as catalysts for the ORR, although they were inactive as anode catalysts. These systems probably can exist with a wide variation in oxygen content. They therefore can readily adsorb oxygen and lose it to the solution after it has been reduced. On the other hand, Armstrong et al. [16] investigated the activity of M_xWO_3 for the ORR and HOR. Steady state current voltage measurements for hydrogen oxidation and oxygen reduction indicated that their activity is too low to be used as catalysts in fuel cells.

2.2. Tungsten carbides

Since the last 1960s tungsten carbide has been considered as an anode material for hydrogen [17] or methanol fuel cells [18]. Binder et al. [17] studied the oxidation of hydrogen on WC electrodes in a H_2SO_4 solution. Hydrogen oxidation occurred at low potential, without affecting the catalyst. Corrosion of the tungsten carbide occurred at potential higher than 300 mV. After corrosion, the electrodes showed only low HOR activity. The behaviour of WC changed significantly after an anodic treatment at about 700 mV in the presence of a reducing agent. Following this treatment, the WC electrode increased its HOR activity, and the corrosion occurred at potentials >700 mV. In these conditions an active layer was formed on the WC surface, likely composed of a hydrogen tungsten bronze, while the inactive surface layer should consist of tungsten oxide. Levy and Boudart [19] reported a platinum-like behavior of tungsten carbide in surface catalysis. On these bases, considering that the surface compositions and chemical states of surface atoms varied with the preparation method, investigations were addressed to the dependence of the HOR activity and stability of high surface area tungsten carbides in acid electrolytes on their preparation method [20–24]. Palanker et al. [20] obtained high surface area tungsten carbide ($30\ m^2\ g^{-1}$) by reduction of high surface area tungstic acid, with subsequent carburization. Polarization curves showed high current densities on high dispersed WC; moreover a substantial

increase in current was achieved by anodic polarization in the range of 300–700 mV in H_2SO_4 under hydrogen. In H_3PO_4, instead, anodic treatment produced a very little effect. At 700 mV, a certain amount of WO_2 (10% of WC content) appeared in the sample. Thus, the current increase on tungsten carbide electrodes after anodic treatment may be due to an increase in the specific activity of the catalyst during oxide formation, and/or an increase in the specific surface area by particle size reduction during oxidation. They found that the increase in the HOR current by anodic treatment in H_2SO_4 involves a simultaneous proportional increase in the catalyst surface, so that the specific activity remains unchanged. Anodic treatment in H_3PO_4 involves no essential change in the catalyst surface and no current increase. Some properties of highly dispersed tungsten carbide differ from those of poorly dispersed WC powder prepared by metallurgists. The composition of metallurgical carbide prepared at about 1500 °C corresponds exactly to that of WC containing 6.12 wt% C, whereas highly dispersed carbide prepared at 750–800 °C contains less than 6 wt% carbon. Palanker et al. [20] compared the specific catalytic activity of metallurgical carbide (SA = 0.1 $m^2 g^{-1}$) with that of highly dispersed (SA = 10–20 $m^2 g^{-1}$) and smooth tungsten carbide. The results indicated no substantial differences between the specific activities of these carbides. Conversely, Ross et al. [21] highlighted the effect of surface composition of tungsten carbides on the activity for hydrogen oxidation. The HOR activity per BET unit area in acid solutions of the carbon deficient, oxygen containing carbides was significantly (about a factor of 3) higher than that of the stoichiometric carbide. This active catalyst was easily prepared by carburizing amorphous, white, tungstic acid hydrate. Oxygen substitution for carbon probably occurred during an intermediate state of carbon dissolution in the reduced tungsten metal and was aided by the defect structure in tungstic acid. According to Ross et al. [21], the increased activity of the oxygen substituted carbide was due to a reduced interaction of the surface with the electrolyte, resulting from covalent tungsten oxygen bonding. However, the HOR activity of tungsten carbide at 25 °C was four orders of magnitude lower than that of Pt. The stoichiometric WC surface was stable in acid electrolyte at anodic potentials of 0–300 mV vs. RHE, but for potentials >300 mV vs. RHE severe oxidation took place. The electrochemically active carbon deficient carbide surface, instead, was stable up to 600 mV vs. RHE. W_2C was much less stable towards oxidation than even stoichiometric WC. The oxygen substitution for carbon with the W–O covalent bond, and not the carbon deficiency itself, produced the stabilization of the carbon surface. Nikolov et al. [22] prepared tungsten carbides starting from different precursors. The carbides investigated were classified in two groups: samples prepared from tungsten oxides and samples synthesized from tungsten and tungstic acid. The activity of the former was half an order of magnitude higher than that of the latter. They concluded that the differences in catalytic activities result from differences in surface properties such as particle morphology and chemical composition, which may significantly differ from that of the bulk. Nikolov and Vitanov investigated the corrosion resistance in H_2SO_4 [23] and the changes in the catalytic activity during corrosion [24] of tungsten carbide synthesized under different conditions. The amount of oxides increased linearly with time, suggesting that during the corrosion process the catalyst surface was not passivated. The corrosion rate depended on the method of preparation of the tungsten carbide. Carbides synthesized from H_2WO_4 and/or at low temperatures displayed the lower corrosion resistance. The different corrosion rates were explained by the variations in the specific surfaces, the grain size, and the different extent of segregation of tungsten carbide particles. During corrosion the specific activity of all the samples reached a maximum after a certain exposure time. The catalytic activity decreased with increase the amount of tungsten oxides formed during corrosion. Corrosion processes lead to some exceptions in the general rule that carbides synthesized from WO_3 display a higher specific activity than those synthesized from H_2WO_4.

Although the performance of tungsten carbide is inferior in direct comparison to platinum [18,21], its low price and its insensitivity to catalyst poisons like H_2S and CO [25,26] make it an interesting alternative to the noble metal catalyst. Thus, in the last decades, tungsten carbides have been tested as alternative Pt electrocatalysts for PEMFCs [27–32], DMFCs [33–43] and MFCs [44–46]. In the following sections various tests of tungsten carbides as catalysts for the use in low-temperature fuel cells are reported.

2.2.1. Tungsten carbides as anode and cathode catalysts for PEMFCs

Polymer electrolyte membrane fuel cells are low-temperature H_2/O_2(air) fuel cells, operating at *ca.* 80 °C that use a proton conducting electrolyte membrane, commonly Nafion®, and Pt or Pt-based catalyst as electrode materials. Yang and Wang [27] tested in a single PEMFC, as the anode material, nanostructured tungsten carbide-based catalysts, synthesized from a stoichiometric mixture of WO_3 and C powders by a mechanical ball-milling process. The synthesized powder was a complex mixture, mainly of hexagonal W_2C and body centered cubic plain W, as well as small amounts of hexagonal WC and solid solutions such as W_6Co_6C, W_3Fe_3C, and W_4Ni_2C. The impurities such as Fe, Ni, and Co were introduced during the mechanical alloying from the miller. Fig. 1 [27] shows the voltage–current polarization curve of the cell with the WC-based anode under fully humidified H_2/air conditions. This PEMFC provided a high current density of 0.9 A cm^{-2} at 80 °C and 3 atm with a low catalyst loading (0.5 mg cm^{-2}). These tests showed the highest electrochemical activity of tungsten carbide catalysts reported to date, and, more importantly, the data were obtained in a real PEMFC.

Brady et al. [28] reported the passivation and electrocatalytic properties of tungsten carbide-based catalysts, synthesized via a solid-state thermal reduction reaction using WO_3 and C as precursors in the W:C atomic ratio 1:1 and 2:1. The synthesis of WC (1:1) gave rise to formation of α-WC, with small amounts of W and W_2C (<2 mol%). The synthesis of WC (2:1) yielded a mixed composition containing WC, W_2C and metallic W, in concentrations of 50, 43 and 7mol%, respectively. The WC (1:1) formed an effective hydrogen oxidation anode. This was attributed to the intrinsic electrocatalytic activity of α-WC, the fine particle size of the material and the clean carbide surfaces formed. The WC (2:1), instead, was a less electrocatalytically active material than WC (1:1) as well as being less passive in H_2SO_4 electrolytes. They proposed that the carbon component itself acts as a passivating agent together with a WO_3 film,

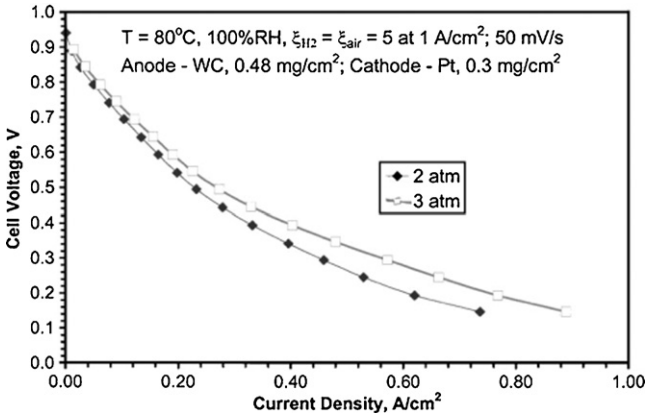

Fig. 1. Polarization curves of the tungsten carbide-based anode in a 5 cm^2 single cell with fully humidified H_2/air at 80 °C. Reprinted from Ref. [27], copyright 2005, with permission from the American Institute of Physics.

accumulating on the carbide surface by dint of tungsten dissolution during passivation. Rees et al. [29] compared the electrocatalytic activity of tungsten carbide synthesized using microwave carburization with that of the carbide synthesized by furnace heating. Microwave apparatus allowed rapid heating and cooling, which was associated with smaller grains of product with higher mass-specific activity for hydrogen electrocatalysis than furnace-heated tungsten carbide.

The effect of the addition of a second metal on tungsten carbide on its catalytic activity was also investigated [29,30,31]. Nagai et al. [30] prepared carbon supported tungsten and nickel-tungsten carbides by carburization of oxide precursors at various temperatures (600–800 °C) and evaluated their HOR activities as anode catalysts in PEMFCs. In the case of WC/C no carbide was formed at carburizing temperature lower than 800 °C. Formation of α-W_2C occurred at a carburizing temperature of 800 °C. For the nickel-tungsten carbide catalysts, the sample carburized at 600 °C contained WO_2 and $NiWO_4$, but no carbides were observed. The carburization of Ni-WC/C at 700 °C produced a mixture of WC and α-W_2C along with a small amount of Ni metal and graphitic carbon. For the Ni-WC/C carburized at 800 °C formation of crystalline WC was observed. The maximum performance of the PEMFC with Ni-WC/C (8.2 mW cm^{-2}) was higher than that of the cell with WC/C (6.4 mW cm^{-2}), but considerably lower than that of the cell with Pt/C as anode catalyst (111.7 mW cm^{-2}). As reported by Rees at al. [29], adding nickel increased the yield of tungsten carbide, to almost 100%. Also, the admixture of nickel into the precursor led to carbides with grain sizes an order of magnitude larger. Conversion of tungsten to tungsten carbide and the growth of WC grains are facilitated by an intermediate phase of nickel tungsten carbide that reduces the activation energy for WC formation. Unlikely than the result of Nagai et al. [30], addition of nickel to WC precursors led to hydrogen oxidation current densities one order of magnitude lower, owing to the reduced surface area of the catalyst [29]. Also the addition of Fe and Mn to WC resulted in a lower activity for hydrogen oxidation. Izhar et al. [31] prepared carbon-supported cobalt-tungsten and molybdenum-tungsten carbides at different carburizing temperatures and tested as anode catalysts in PEMFCs. For the Co-WC carburized at 600 °C, formation of a CoW alloy, $CoWO_4$ and Co_6W_6C phases, and an (oxy)carbidic phase was observed. The Mo-WC carburized at 600 °C contained only MoO_2 and WO_2. The surface areas of Co-WC were one magnitude lower than those of Mo-WC. The Co-WC catalyst carburized at 600 °C exhibited the highest maximum power density compared to Mo-WC and WC catalysts. According to the authors, the presence of oxycarbided and/or CoW was responsible for the enhanced HOR activity of Co-WC.

It is very difficult to use a pure tungsten carbide as cathode electrocatalyst in PEMFCs, because this material has a very low corrosion resistance under acidic and oxidative conditions. When tungsten carbides are used as cathode catalysts, these materials must be modified to improve both the stability and the electrocatalytic activity in a highly corrosive atmosphere. To increase the stability of tungsten carbides, the addition of a second metal to carbides was investigated [32]. Lee et al. [32] studied the effect of Ta addition to WC with respect to the stability and ORR activity. They found that the corrosion resistance of the tungsten carbide was significantly increased by the addition of Ta. The ORR activity of the Ta-WC catalyst was 0.35 V higher than that of the pure WC catalyst. Formation of a WTa alloy was considered. The WTa alloy might increase the stability of the WC in an acid electrolyte. The enhanced electrocatalytic activity might be due to the presence of tungsten carbide, which existed on the surface and/or sub-surface.

2.2.2. Tungsten carbide as anode catalyst for DMFCs

Direct methanol fuel cells are low-temperature fuel cells similar to PEMFCs, but fuelled with methanol. Generally, tungsten carbide has been reported to show promising electrochemical properties for the methanol oxidation reaction (MOR) [33–43]. As previously reported, the activity of WC for hydrogen oxidation was related to the carbon deficiency and oxygen replacement in carbon layers of the WC lattice [21]. However, the role of oxygen in WC for methanol oxidation can be different from that for hydrogen oxidation. Okamoto et al. [33] investigated the state of oxygen in WC and its effect on the MOR. They prepared WC by carburization of WO_3 with CO at 700 °C for different times to obtain WC with a variety of carburization levels. As carburization proceeded, WO_3 was reduced to WC through $W_{18}O_{49}$ and WO_2, and the specific surface area increased. C/W and O/W atomic ratios increased and decreased, respectively, as carburization proceeded. They found that the surface was in a more oxidized state than bulk. With WC(6) (the number in brackets indicates the carburizing period), tungsten oxides disappeared and only the WC phase was present. WC(6) showed the maximum MOR activity. When the carburization period was too short, the sample was not fully carburized, and when the carburization period was too long, free carbon accumulated on the surface, which is poisonous. However, for hydrogen oxidation, WC(5) provided maximum activity. This indicates that the active sites for methanol oxidation are different from those for hydrogen oxidation. WC(6) with maximum activity for methanol oxidation possessed oxygen as much as 0.25 in O/W. This oxygen is considered to be present in the WC lattice. They also found that, when WC samples are heated in an atmosphere of He or H_2, its catalytic activity is enhanced to the maximum of all the samples. Since the sample heated in He includes very little oxygen, it is strongly suggested that much oxygen in the WC lattice does not play an important role in methanol oxidation. Kawamura et al. [34] investigated the MOR activity in H_2SO_4 of WC and tungsten-based double carbides [(W,M)C; M = V, Cr, Mn, Ni and Mo]. Only Mo was able to promote the MOR activity. After optimizing the preparation method of carbides, the most active catalyst for methanol oxidation was (W,Mo)C synthesized at 700 °C with the atomic ratio Mo/(W + Mo) = 0.2. Corrosion current is almost negligible at potentials up to 0.55 V. Fig. 2 [34] shows the variation in the MOR activity for both alkaline untreated and treated carbides with Mo content. The MOR activity increases remarkably even at a Mo content such as 0.01. The MOR activity reaches a maximum between 0.1 and 0.2 of Mo content and then gradually decreases as the content increases. When Mo content exceeds 0.2, formation of the β-Mo_2C phase occurred, and β-Mo_2C amount increased with increasing Mo

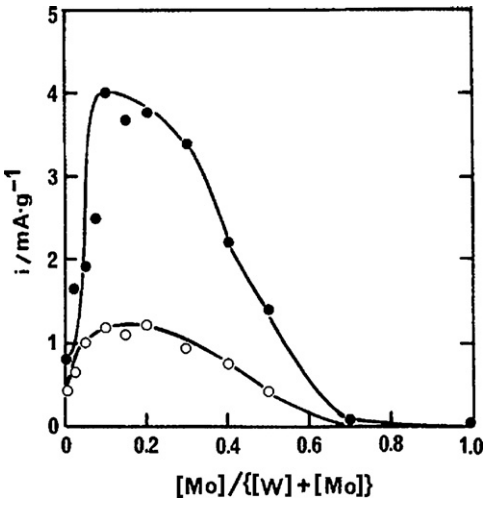

Fig. 2. Effect of Mo content on methanol oxidation activity of (W,Mo)C. (●) and (○) indicates with and without alkaline treatment, respectively. Carburizing temperature: 700 °C. Reprinted from Ref. [34], copyright 1987, with permission from The Electrochemical Society.

content. The decrease in catalytic activity for Mo content >0.2 was likely due to the formation of β-Mo_2C.

Hwu et al. [35–38] studied the reactions of CH_3OH, H_2O and CO over several tungsten carbide surfaces. They demonstrated that methanol and water readily dissociate on C/W(1 1 1), Pt/C/W(1 1 1), O/C/W(1 1 1), and C/W(1 1 0). When the C/W(1 1 1) surface is modified by oxygen, significant activities toward the decomposition of methanol and water are maintained while the CO desorption temperature is reduced to below room temperature. Overall, they observed that tungsten carbide surfaces exhibit characteristics more favorable toward DMFC applications than Pt or Ru surfaces in two important aspects: (1) the tungsten carbide surfaces are more active toward the dissociation of methanol and water and (2) the CO desorption temperature is at least 100° lower, suggesting that tungsten carbides might be more resistant to CO poisoning. Weigert et al. [39] evaluated the activity and stability of Pt, WC and Pt-modified WC thin film surfaces in H_2SO_4/CH_3OH solution. On pure Pt, methanol underwent a single oxidation state during the positive sweep of CV. The CV curve of methanol oxidation on the Pt foil showed an onset beginning at ~0.7 V, with a maximum oxidation current of 0.2 mA cm^{-2} occurring at ~0.9 V vs. NHE. The decline of this oxidation feature coincided with the onset of Pt oxidation. On the negative sweep of the CV curve, an increase in the current was observed with a feature centered at ~0.7 V, resulting from surface poisoning by intermediates formed during the methanol oxidation. Similar to the Pt surface, the CV curve of methanol oxidation on WC showed a single oxidation state. However, the onset of methanol oxidation occurred at a lower voltage than that on Pt, beginning at ~0.5 V. The maximum current of ~0.3 mA cm^{-2} occurred at ~0.65 V, just prior to the onset of WC oxidation into W_xO_y species. Unlike Pt, the negative sweep of the CV curves on WC did not display any additional features. This was attributed to the weaker interactions of surface intermediates, in particular CO, with the WC and Pt-modified WC surfaces. However, the WC surface underwent partial oxidation after repeated CV cycles, as indicated by XPS measurements and by the decrease in the oxidation current at 1.0 V from the 1st to the 30th cycle. Very recently, Lu and Yan [40] prepared WC microspheres by reduction and carbonation of WO_3 microspheres. WC was the only phase present in the sample. The grain size of WC was from about 20 to 100 nm. Unlikely than WO_3 microspheres, WC microspheres showed electrocatalytic activity for methanol oxidation, but much lower than that of Pt.

Regarding the products of methanol oxidation on WC different results are reported in literature. Miyasaki et al. [41] investigated the catalytic decomposition of methanol on the transition metal carbides TiC, TaC, Mo_2C, W_2C, and WC. On WC methylformate was produced with high selectivity (>80%), whereas other catalysts produced mainly CO and H_2. On the contrary, more recently, Angelucci et al. [42] investigated the methanol oxidation on WC by differential electrochemical mass spectroscopy (DEMS). Measurements of DEMS showed that the methanol oxidation reaction over tungsten carbide produces CO_2. No methylformate was detected.

Conversely to the previous investigations, Barnett et al. [43] observed no MOR activity on WC. They studied the MOR on WC and Ni-WC. Whilst WC is highly passive (the passive current densities are comparable with the Ni-WC), no electrocatalytic activity towards methanol oxidation was detected. MOR activity would thus require the presence of Ni dissolved in the WC matrix.

2.2.3. Tungsten carbide as anode catalyst for MFCs

Microbial fuel cells are electrochemical devices that convert the chemical energy contained in organic matter into electricity by means of the catalytic (metabolic) activity of living microorganisms. A type of MFC is based on the direct oxidation of reduced, energy-rich metabolic products (primary metabolites) that are formed, e.g., during a fermentative substrate degradation. For microbial fuel cell application, an electrocatalyst should possess good biocompatibility (no microbial toxicity), high electrocatalytic activity towards the oxidation of various metabolites, electrocatalytic activity at low temperatures (10–40 °C), electrocatalytic activity at pH between 5 and 7, chemical and electrochemical stability as well as high stability against biofouling, insensitivity against poisoning by biological products and low costs. Tungsten carbide fulfills the requirements for a MFC anode catalyst. It also possesses the ability to catalyze several different pathways for the oxidation of inorganic and organic metabolites, for example, hydrogen and formate. This is of prime importance for achieving high conversion efficiencies. Rosenbaum et al. [44] proposed a high performance, completely noble-metal-free, microbial fuel cell based on tungsten carbide as anodic electrocatalyst. The results indicated that tungsten carbide is suitable as anodic electrocatalyst for MFC application. At WC-modified graphite electrodes, current densities of up to 3 mA cm^{-2} were achieved in hydrogen saturated synthetic electrolytes (phosphate buffer). Further, a microbial fuel cell based on soil bacteria as biocatalysts and tungsten carbide as anodic electrocatalyst delivered the highest so far reported MFC power density of 586 μW cm^{-2}. In a next paper, Rosenbaum et al. [45] evaluated the electrocatalytic activity of tungsten carbide in the light of its preparation procedure, its structural properties as well as the pH and the composition of the anolyte solution. The activity of WC towards the oxidation of several common microbial fermentation products (hydrogen, formate, lactate, ethanol) was studied in MFC conditions (e.g., pH 5, room temperature and ambient pressure). Tungsten carbide was synthesized using two different preparation methods: WC I was prepared via the carburization of WO_3 in a CO atmosphere at 800 °C. WC II was prepared similarly to WC I, but a powder mixture of WO_3 with $H_2C_2O_4$ and NH_4Cl was used. The synthesis was performed at 750 °C. XRD patterns of both samples showed only reflections of WC, with no visible peaks of W_2C, W or WO_2. Current densities of up to 8.8 mA cm^{-2} were achieved for hydrogen, and up to 2 mA cm^{-2} for formate and lactate, respectively. No activity was observed for ethanol electrooxidation. WC II showed a considerably higher catalytic activity for hydrogen oxidation than WC I. The grain size and the physical surface area of all samples were similar and no correlation can be derived between the catalytic activity and the phase composition. A texturing of the powder samples, possibly caused by a deviation of the crystal shape from the statistical average, appears to lead to a decreased electrocatalytic activity of WC I. The electrocatalytic activity and chemical stability of WC was excellent in acidic to pH neutral potassium chloride electrolyte solutions, whereas higher phosphate concentrations at neutral pH supported an oxidative degradation. These results indicated that tungsten carbide is a promising MFC electrocatalyst, capable of efficiently oxidizing common fermentation products like hydrogen, formate and lactate under the conditions of microbial fuel cells. Conversely, Harnisch et al. [46] demonstrated the complexity of the electrochemical and electrocatalytic properties of tungsten carbide for the use in MFCs. They showed that pure WC may not be advantageous for MFC application, since WC preferably oxidizes hydrogen, with low ability to oxidize organic metabolites such as formate and lactate. The additional presence of W and W_2C phases can improve the catalytic activity towards these compounds, and can thus improve the efficiency of the anodic metabolite oxidation. A problem to be solved is the liability of the catalyst to corrosion at pH neutral conditions, which leads to a slow but continuous dissolution of the catalyst.

2.3. Tungsten nitrides

Transition metal carbides, as tungsten carbide and molybdenum carbide, are not suitable as cathode catalyst for acidic fuel cells,

owing to their low corrosion resistance under acidic and oxidative conditions. The transition metal nitrides, instead, are chemically inert in acidic solution at cathodic potentials, so their use as cathode catalysts has been investigated. Zhong et al. [47] prepared carbon supported tungsten nitride and investigated its ORR activity for a possible use as a fuel cell cathode catalyst. XRD pattern of the tungsten nitride showed the characteristic reflexions of the fcc β-W_2N compound. The W_2N/C catalyst presented good electrocatalytic activity for the ORR. The onset potential for the ORR on the electrode modified by the W_2N/C catalyst occurred at a relatively positive potential as a non-noble catalyst, about 0.6 V, although it was still negative than that of Pt/C. This catalyst was tested in a single PEMFC at various temperatures. The maximum power densities were 16.0 mW cm^{-2} and 39.2 mW cm^{-2} at 60 and 80 °C, respectively. Stability test for the W_2N/C electrocatalyst was carried out at the current density of 120 mA cm^{-2} under fuel cell conditions. The single cell output voltage maintained almost at the same value during the test time (100 h). The high stability of the catalyst may be due to the high stability of the tungsten nitride itself in low potential and the presence of WO_2 on the surface maybe also increased the activity and the stability of the catalyst.

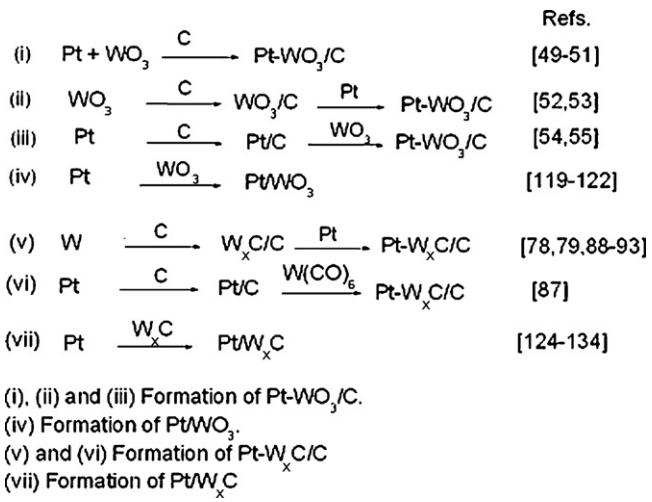

Fig. 3. A representative scheme of the formation of Pt-WO_3/C, Pt/WO_3, Pt-W_xC/C and Pt/W_xC.

3. Tungsten-based materials as anode and cathode co-catalysts

3.1. WO_x as co-catalyst in Pt-WO_x

Dispersed noble metal nanoparticles supported on high-surface-area oxides are of considerable interest to catalysis. One of the functions of the support is to separate the particles physically to diminish the rate of their degradation by agglomeration. Inorganic oxides can also influence supported metal centers in other ways, e.g., by affecting their chemisorptive and catalytic properties. Efficient electrocatalytic systems would involve mutual metal-support interactions leading to activation of both dispersed metal and oxide matrix toward electrode processes. WO_x fulfills the requirements of an effective catalyst support [48]. Generally, Pt-WO_x systems are formed by co-deposition of Pt and WO_x precursors on the support [49–51], commonly high surface area carbon. When used in fuel cells, to increase WO_x surface area, before Pt dispersion, tungsten oxide is supported on carbon [52,53] or, to increase Pt dispersion, WO_x is deposited on preformed Pt/C [54,55]. In some cases, WO_x is used as carbon-alternative catalyst support. The use of tungsten oxide as carbon-substitute substrate for fuel cell catalysts will be discussed in Section 4. A representative scheme of the formation of Pt-WO_3/C and Pt/WO_3 is reported in Fig. 3.

3.1.1. Early studies on Pt-WO_x as catalyst for hydrogen and methanol oxidation

Firstly, Benson et al. [56] observed that the reduction of WO_3 by H_2 to a blue form proceeds readily above 400 °C. If the WO_3 powder is mixed with platinum black, reduction will start below 100 °C. But if this mixture is made to adsorb water, reduction takes place rapidly at room temperature. The catalysis by platinum is apparently due to the dissociation of molecular hydrogen on the metal, followed by diffusion of adsorbed hydrogen atoms across the metal-oxide interface. The acceleration by water was ascribed to a marked increase in the rate of diffusion of the reducing species. Hobbs and Tseung [57] proposed an alternative explanation in which WO_3, in physical contact with Pt, participates in the electrode reaction via formation of hydrogen tungsten bronzes (H_xWO_3):

$$WO_3 + x\text{Pt-H} \rightarrow H_xWO_3 + x\text{Pt} \rightarrow WO_3 + xe^- + xH^+ + x\text{Pt} \quad (1)$$

H_xWO_3 is formed in platinized WO_3 under the prevailing conditions in a fuel cell hydrogen electrode. The highest degree of reduction, $H_{0.44}WO_3$, was obtained at 25 °C using an impregnation technique for platinizing with 0.8 wt% Pt. Mechanical mixtures do not produce very intimate mixing, resulting in slower, incomplete reduction which can be improved by increasing the Pt loading. So long as the electrolyte is acidic, pH has no effect on the reduction [58]. Hydrogen bronzes, formed in platinized WO_3 hydrogen electrodes, contribute to the net anodic current, being formed chemically by H-atom migration from the Pt to the oxide, and oxidizing electrochemically. Thus, the reaction zone is extended onto the support and the over-all electrode activity is increased. With Pt loadings in the range of 0.02–0.1 mg cm^{-2} (or 0.2–1% of the WO_3 loading) high electrode performance was obtained which originated principally from the bronze reaction. The rate of hydrogen atom migration to form bronzes is rapid provided there is direct contact between Pt and WO_3 particles. Hydrogen atom migration between oxide particles is relatively slow and, under conditions where this is necessary for current generation, a severe decline in activity is observed [59]. Initial performance of the platinized lower tungsten oxide (WO_x, where $2 < x < 3$) electrodes is lower than the corresponding WO_3 electrodes. However, their performance improves with time as the surface is converted to WO_3 rich layers until a limiting thickness is reached. The bulk of the lower tungsten oxide is then protected from further oxidation and does not participate in the over-all electrode reaction [60].

Pt-WO_3 systems showed also more tolerance to CO presence and higher activity for methanol oxidation than Pt alone. Teflon bonded electrodes using mechanically mixed Pt black and WO_3 powder have been reported to be less susceptible to carbon monoxide poisoning in H_2/CO mixtures, since water adsorbed on the tungsten oxide surface can interact with CO adsorbed on adjacent platinum sites [61]. Kulesza and Faulkner [62] observed that in Pt-WO_3 the MOR activity of platinum was enhanced by reductive conditioning at −0.2 V vs. SCE, where hydrogen spillover from Pt to yield hydrogen tungsten bronzes takes place. This process was believed to be responsible for the removal of passivating methanol residues, presumably by desorptive hydrogenation.

3.1.2. Recent studies on Pt-WO_x and Pt-Ru-WO_x catalysts for H_2/CO and CH_3OH oxidation

Many works in the 1990s and 2000s have been addressed to binary Pt-WO_3 and ternary Pt-Ru-WO_3 for the HOR/CO and the MOR. Generally the catalytic activity of Pt-WO_3 for hydrogen and methanol oxidation was higher than Pt but lower than Pt-Ru [49–54,63–68]. The activity of ternary Pt-Ru-WO_3, instead, was

higher than both Pt and Pt-Ru [55,66,68–73]. Zhou et al. [74] tested Pt-WO_3 and Pt-Ru-WO_3 for the ethanol oxidation reaction (EOR) and compared their EOR activity with that of Pt, Pt-Ru and Pt-Sn. The EOR activity increased in the order Pt < Pt-WO_3 < Pt-Ru < Pt-Ru-WO_3 < PtSn. The question is whether the enhanced HOR and MOR activity and CO tolerance of the WO_x containing catalysts are due to the improved catalytic properties or to the change of the physical characteristics of the catalyst such as particle size and surface area. Shen and Tseung [63] concluded that the advantages of using Pt-WO_3 electrodes for methanol oxidation would be keeping the Pt sites clean for chemisorption of methanol by the continuous formation and oxidation of H_xWO_3 during the dehydrogenation of methanol on the surface of the Pt-WO_3 electrode, and active for the oxidation of poisons, such as CO, since water adsorbed on WO_3 surface interacts with the CO adsorbed on Pt at the adjacent Pt-WO_3 sites. The fact that the Pt-WO_3 electrodes perform best at low acid solutions is further evidence that the rate-determining step is the supply of OH_{ad}, since the dehydrogenation of methanol is fast in the presence of WO_3. Shukla et al. [64] assumed that the WO_x is present in the form of an oxyhydroxide, which can promote surface oxy-species on platinum by proton transfer, with a rapid change of the oxidation state of W, involving the redox couple W(VI)/W(IV). In agreement with Shukla et al. [64], Jayaraman et al. [51] speculated that tungsten changes oxidation states between +6 and +5, providing the oxygen species required for the removal of CO. The XPS results showed the presence of small amounts of W^{5+} in addition to W^{6+}. Colmenares et al. [65] explained the high HOR activity of Pt-WO_x in the presence of CO by a combination of several effects, i.e., a high HOR activity on the unmodified Pt surface areas, an improved activity of the WO_x deposit for the generation of oxygen species and reaction with CO_{ad} on neighboring Pt sites, and a low mobility of CO_{ad} species, leaving CO_{ad} free Pt areas for the HOR around the deposited WO_x islands.

On the contrary, other studies attributed the increase activity of Pt to physical effects rather than any catalytic effects of WO_3. As reported by Shim et al. [54], in Pt-WO_3/C, the active surface area, obtained by hydrogen desorption, increased with increasing WO_3 content. The total charge for hydrogen desorption includes the formation of H_xWO_3. When the coulombic charge for formation of H_xWO_3 is removed from total charge, the electrochemically active surface area slightly decreases with increase of WO_3 amount over 10%, but is still higher than pure platinum. According to Yang et al. [66], the addition of tungsten to Pt-Ru appeared to mainly result in some 'physical' modification of the catalytically active Pt and Ru surface components such as differences in electroactive surface area rather than promotion of the MOR via a true catalytic mechanism. The MOR activities per Pt + Ru surface area were very similar for a particular set of catalysts, that is, Pt/C vs. PtWO_x/C and PtRu/C vs. PtRuWO_x/C. This suggested that WO_x does not exhibit a true catalytic activity for methanol oxidation. This is consistent with the i/V shape and CH_3OH onset potential obtained from the slow sweep CVs that were essentially identical for the Pt/C vs. PtWO_x/C and PtRu/C vs. the PtRuWO_x/C catalysts.

A comparative study of experimental and theoretical combinatorial and high-throughput screening methods for the development of novel materials was presented by Strasser et al. [75]. Both methods were applied to the development of Pt-based anode fuel cell catalysts with improved CO tolerance. Most W-containing compositions, with the molar fractions of all three base metals ($x_W + x_{Co} + x_{Ni}$) roughly equals 0.5–0.6, showed very low to no current activity. However, there was a group of very active W-containing, Ru-free compositions with a combined base-metal molar fraction ($x_W + x_{Co} + x_{Ni}$) of about 0.8. Due to their high base metal content, these compositions underwent strong surface corrosion and surface roughening during the pretreatment leading to high current densities due to their increased surface area. These active W-containing compositions appeared to corrode more severely and showed reduced specific activity after correction for their surface area. While a few W-containing catalysts still maintain activities comparable or slightly better than the standards, their longer term stability remains questionable.

Jayaraman et al. [51] investigated the effect of WO_3 content on the MOR activity of Pt-WO_3 catalysts. Fig. 4 [51] shows the MOR activity of the Pt-WO_3 system as a function of Pt content. Fig. 4a shows the methanol oxidation current density vs. % Pt at 0.6 and 0.8 V vs. RHE. The current densities measured at 0.8 V are much higher than those at 0.6 V, due to the onset of surface oxides on Pt at 0.8 V, which facilitate oxidative removal of carbonaceous surface poisons, and the extra 0.2 V supplied to drive the oxidative reaction. From Fig. 4a, one can qualitatively observe that Pt-WO_3 catalysts with Pt contents greater than 50% possess higher activity than pure Pt, both at 0.6 V and at 0.8 V. This improvement in performance is quantified in Fig. 4b, which normalizes the activity of each catalyst versus pure Pt. Although the measured oxidative current densities for Pt-WO_3 catalysts are lower at 0.6 V than those at 0.8 V (Fig. 4a), Fig. 4b demonstrates that at 0.6 V the effect of WO_3 is more pronounced than at 0.8 V.

Pereira et al. [67] investigated the performance of PEMFCs fed with H_2/CO for anodes with Pt-WO_x/C and $H_3PW_{12}O_{40}$-impregnated Pt/C electrocatalysts. A quite higher performance was achieved for the PEMFC fed with H_2 + 100 ppm CO with anodes containing Pt-WO_x/C and also for those with $H_3PW_{12}O_{40}$-impregnated Pt/C than that of the cell with Pt/C alone. A decay of the single cell performance with time was observed, and this was attributed to an increase of the membrane resistance due to the polymer degradation promoted by the crossover of the tungsten species throughout the membrane. The stability of WO_3 in acid medium can be improved by suitable substitution of transition metal ions into the oxide framework [76]. Raghuveer and Viswanathan [52] increased the stability of WO_3 by addition of titanium ions to tungsten oxide. The improvement in the stability could be due to the alteration in the rate of hole capturing process of WO_3 by the Ti^{4+} at the interface, which is responsible for the dissolution of tungsten in acidic solution. However, the improvement in WO_3 stability was obtained only when titanium is present in low amounts. At higher Ti^{4+} content, the Ti^{4+} is no longer stable in the oxide framework, which undergoes reduction during the hydrogen treatment. The electrocatalytic activity for methanol oxidation followed the order: Pt-$W_{0.83}Ti_{017}O_3$/C > Pt-WO_3/C > Pt-$W_{0.91}Ti_{0.09}O_3$/C ~Pt-$W_{0.95}Ti_{0.05}O_3$/C. The trend in the activity observed correlates well with that of the increase in the ohmic resistance of the electrode.

3.2. Metal-tungsten carbide composite catalysts

As in the case of WO_x, various papers report the use of tungsten carbide dispersed on a high surface area carbon (WC/C or W_2C/C) as catalyst support: to increase its surface area, tungsten carbide is synthesized on a carbon support and then the metal catalyst is deposited onto this mixed substrate [77–79]. As we will discuss in the Section 4, W_xC is also used as carbon-alternative catalyst support. A representative scheme of the formation of Pt-W_xC/C and Pt/W_xC is reported in Fig. 3. The high surface area of carbon-supported tungsten carbide enhanced the interactions between tungsten carbide and the metal catalyst, and, as a consequence, the catalytic activity of the composite material, owing to the increased synergic effect. Metal-tungsten carbide composite catalysts have been tested for different reaction, such as hydrogen, methanol, formic acid and ethanol oxidation and oxygen reduction. Firstly, Wolf et al. [80] investigated the activity of WC by incorporating small amounts of platinum into the WC substrate. The incorporation was done by ion implantation and ion beam mixing. The results indicated that the implanted substrates are much more

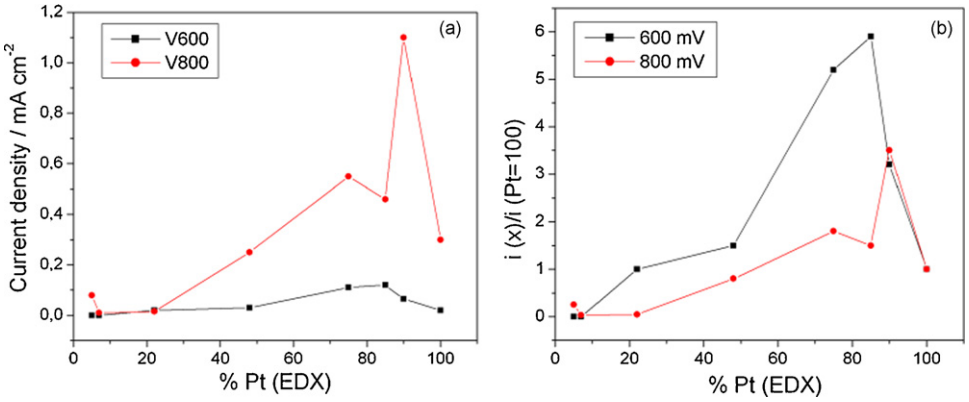

Fig. 4. Methanol oxidation activity plots for the Pt-WO_3 system as a function of Pt composition at two different potentials: 0.6 V and 0.8 V vs. RHE. (a) Current density at 300 s for 0.6 V data and at 600 s for 0.8 V data as a function of the Pt composition. (b) Normalized current density as a function of Pt composition. The curves were obtained by dividing the current density of each of the samples with that of the corresponding current density of the 100% Pt sample. Reproduced from Ref. [51], copyright 2005, with permission from the American Chemical Society.

active for methanol and formic acid oxidation than the untreated ones, and above a dose of 1016 Pt^+ cm^{-2} the activity even exceeds the one of smooth platinum metal. Ion beam mixing was less effective. Implantation of Pt into WC causes the formation of very small Pt-clusters, which interact electronically with the substrate, giving rise to the superior catalytic activity. This view was supported by long term measurements. While smooth platinum was easily poisoned by reaction intermediates or by-products, the Pt-implanted WC was not. Either the adsorbed by-products were more easily oxidized and desorbed or because of different adsorption strength the by-products were formed to a much lesser extent.

Liu et al. [81] studied the bonding and dissociation of methanol, water, and hydrogen on submonolayer Pt-modified C/W(1 1 1) surfaces using high-resolution electron energy loss spectroscopy (HREELS) and temperature-programmed desorption (TPD). The decomposition pathways of methanol on C/W(1 1 1) are significantly modified by the presence of submonolayer coverages of Pt. On the unmodified C/W(1 1 1) surface, the decomposition of methanol occurs via three pathways: partial decomposition to produce CO and H_2 (~31% selectivity), partial decomposition to form methane and atomic oxygen (~14% selectivity), and complete decomposition to produce hydrogen, atomic carbon, and atomic oxygen (~55% selectivity). In contrast, on the Pt/C/W(1 1 1) surface, ~49% of methanol partially dissociates to CO and H_2, and the other ~51% of methanol undergo complete decomposition to hydrogen, atomic carbon, and atomic oxygen. The presence of submonolayer coverages of Pt prohibits the production of methane, which is an undesirable side product in DMFCs. Furthermore, both the C/W(1 1 1) and the Pt/C/W(1 1 1) surfaces are active toward the dissociation of hydrogen and water. However, the amount of adsorbed water that undergoes dissociation is reduced from 0.18 H_2O per W atom on C/W(1 1 1) to 0.056 H_2O per W on Pt/C/W(1 1 1). Zellner and Chen [82] also investigated the reaction of methanol on WC films modified by low coverages of Pt: they found a promoting effect of Pt for the dissociation of methoxy in the temperature range 673–773 °C. As previously reported, Weigert et al. [39] evaluated the activity and stability of WC, Pt-WC, and Pt thin film surfaces in H_2SO_4/CH_3OH solution. The Pt-WC surface showed methanol oxidation CV curves similar to those of the WC surface, with an enhancement in the stability of the electrocatalysts, as indicated by XPS measurements and by the similar CV curves from the 1st and 30th cycles. Mellinger et al. [83] found that the combination of low coverages of Pt with WC results in a synergistic effect for the oxidation of CO, leading to a higher activity than Pt and higher stability than WC. In agreement with Mellinger et al. [83], Zhao et al. [84] ascribed the high activity for methanol oxidation on multi-walled carbon nanotubes supported Pt-WC catalysts to the easier oxidation of CO-like species by the synergistic effect between Pt nanoparticles and WC, which could reduce the overpotential for CO oxidation. The promising properties of Pt-WC suggest the possibility of utilizing these materials as CO-tolerant electrocatalysts.

Scanning electrochemical microscopy (SECM) was used to rapidly screen thin film composition gradient materials libraries for their electrocatalytic activity towards hydrogen oxidation and CO tolerance. Binary and ternary Pt-based catalysts were investigated as anodic materials for PEMFCs by Cooper et al. [85]. They observed that, for most ternary Pt-Ru-WC compositions, the addition of WC to Pt-Ru catalysts can improve their HOR activity and CO tolerance. SECM screening suggests Pt-Ru-WC and Pt-WC can be potential electrocatalysts for PEMFCs. The approximate optimum composition was $Pt_{25\pm10}Ru_{5\pm5}(WC)_{70\pm5}$ for the ternary library, and 65–80 at% WC for the binary Pt-WC library.

Both hexagonal α-WC and cubic β-WC structures showed a synergic effect, with Pd for ethanol oxidation and with Pt for hydrogen oxidation, respectively. Hu and Shen [86] compared the EOR activity in alkaline media of Pd-α-WC/C with that of Pd/C. Hexagonal α-WC nanocrystals, with particle size about 20 nm, were prepared by an intermittent microwave heating (IMH) technique. The Pd-α-WC/C electrocatalyst showed a higher EOR activity compared to that of Pd/C with a more negative onset potential and higher peak current densities. Kim et al. [87] prepared multiwalled carbon nanotube-supported Pt-β-WC catalysts. The β-WC nanoparticles were prepared by a sonochemical method with a $W(CO)_6$ precursor. The sonochemical technique has the advantage of forming β-WC nanoparticles, which are the most active among the tungsten carbide phases. These materials exhibit enhanced HOR characteristics with Pt-specific mass activities about twice than that of pure Pt.

In all the above-mentioned works, the metal-tungsten carbide composites were tested only as anode materials. Ticianelli et al. [78] and Jeon et al. [79], instead, tested Pt-W_xC both as anode and cathode materials for use in PEMFCs. Ticianelli et al. [78] used tungsten carbide dispersed on a high surface area carbon (W_2C/C) as platinum support. The Pt-W_2C/C catalyst was tested for the ORR and HOR in acid medium. Pt-W_2C/C showed a remarkable enhancement of the ORR, when compared to Pt/C, both following a four-electron mechanism. Pt-W_2C/C and Pt/C showed similar HOR activity and kinetics, following the direct discharge mechanism on both catalysts. Jeon et al. [79] investigated the activity for methanol oxidation and oxygen reduction of a Pt/WC/C catalyst. WC was synthesized on a carbon support and then Pt was deposited to obtain a Pt-WC/C catalyst. Pt-WC/C showed a 42% higher specific activity for MOR and a 170% higher current density for the ORR compared with those of

Pt/C. In addition, a superior ORR current density was maintained in the presence of methanol.

Regarding the oxygen reduction, the group of Shen addressed a lot of papers to the ORR on M-WC/C catalysts (M = Pt, Ag, Pd)) both in acid and, particularly, in alkaline media [88–93]. Firstly, Meng and Shen [88] prepared W_2C and W_2C-modified Pt catalysts by IMH and tested their ORR activity in alkaline media. As shown in Fig. 5 from ref. [87], the W_2C nanocrystals were active towards oxygen reduction. The ORR on Pt/C reduced the overpotential by 150 mV compared with that on the pure W_2C catalyst. The activity for the ORR was further improved on a Pt-W_2C/C catalyst at a lower Pt loading. As can be seen in Fig. 5, the potential shifted towards the positive side more than 50 mV on Pt-W_2C/C than on Pt/C at a reasonable reduction current density. Thus, the current density could be ten times larger on Pt-W_2C/C than that on Pt/C operating at cathodic potentials. Moreover, the effect of methanol presence on the performance of ORR on the Pt-W_2C/C electrode was less severe than on Pt/C, suggesting a potential application of Pt-W_2C/C as cathode catalyst in alkaline DMFCs. In similar works, the activity for the ORR in alkaline media of Pt-free Ag-W_2C/C [89] and PdAu-W_xC/C (here W_xC is a mixture of W_2C and WC) [90] catalysts was also investigated. Ag-W_2C/C showed similar ORR activity to that of Pt-based electrocatalysts, while PdAu-W_xC/C presented higher ORR activity than PdAu/C and Pt/C. Meng and Shen [91] prepared carbon-supported tungsten carbide with different W/C ratio by IMH. The average particle sizes were < 10 nm for W/C weight ratios <30 wt%, while the particles grow bigger at higher ratios. The particle size exceeds 20 nm at W/C = 50 wt%. Formation of pure W_2C occurred at W/C <30 wt%. Further increase in the content of W resulted in the formation of WC. The ratios of WC to W_2C increased with increasing the heating time. They tested the ORR activity of Pt-W_2C/C [91] and Pt-W_xC/C [92] in acid media. Both Pt-W_2C/C and Pt-W_xC/C showed much higher ORR activity than Pt/C. In a next work [93], Shen et al. tested Pt-W_2C/C as cathode catalyst in a single DMFC. Fig. 6 [93] shows the performance of DMFCs using Pt/C and Pt-W_2C/C as cathode catalysts. The open circuit potential of the cell with the Pt-W_2C/C composite cathode was 0.84 V, which is 0.13 V higher than that of the cell with Pt/C. The maximum power density of the cell with Pt-W_2C/C was 36% higher than that of the cell with Pt/C, with a much higher Pt loading.

Recently, Wang et al. [94] designed an i*n situ* simultaneous synthesis of WC/graphitic carbon (WC/GC) nanocomposites. They prepared a WC/GC composite by using polyacrylic weak-base anion exchange resin as carbon source. The fabrication procedures start with introduction of WO_4^{2-} and $[Fe(CN)_6]^{4-}$ ions into the raw resin, forming a resin-WO_4^{2-}-$[Fe(CN)_6]^{4-}$ complex. WO_4^{2-} and

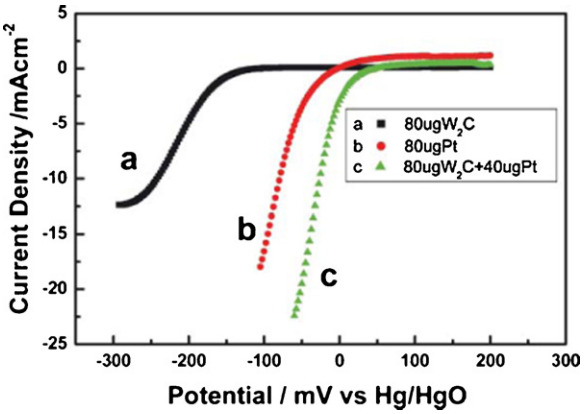

Fig. 5. Linear potential sweep curves of W_2C/C, Pt/C and Pt-W_2C/C for oxygen electroreduction. Reprinted from Ref. [88], copyright 2005, by permission of The Royal Society of Chemistry.

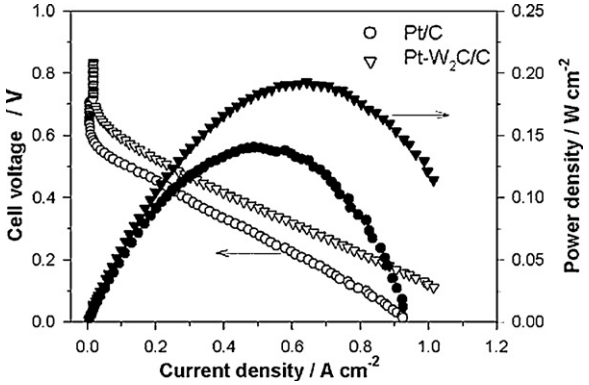

Fig. 6. Comparison of the performance of a single DMFC at 90 °C. Anode: 40% PtRu/C (Pt/Ru loading = 3.0 mg cm^{-2}); cathode: 40% Pt/C (Pt loading = 3.0 mg cm^{-2}) and Pt-W_2C/C (W_2C:Pt = 2:1, Pt loading = 1.0 mg cm^{-2}). Reprinted from Ref. [93], copyright 2006, with permission from The Electrochemical Society.

$[Fe(CN)_6]^{4-}$ were used as tungsten precursor and graphitization catalyst, respectively. After being carbonized under nitrogen atmosphere at 1000 °C for 1 h, the resin polymer was converted into graphitic carbon; meanwhile, the tungsten precursor was *in situ* reduced to form WC that is intimately incorporated with the carbon phase. Such an intimate contact between the active component and carbon is favorable for high catalytic activity and stability. Following removal of Fe species, the WC/GC composite was obtained. Then, Pt was loaded on WC/GC by the $NaBH_4$ reduction method with a loading of 7.5 wt%. CV for methanol oxidation at Pt-WC/GC and Pt/C showed a similar peak potential at about 0.71 V. However, the Pt-WC/GC catalyst exhibited a substantially higher mass activity of 205.6 mA mg^{-1} Pt and a lower onset potential of 0.24 V, compared with 62.3 mA mg^{-1} Pt and 0.30 V for the Pt/C catalyst, indicating that the Pt-WC/GC catalyst possesses higher MOR activity than Pt/C.

3.3. M-W (M = Pt, Pd) and M-Ru-W (M = Pt, Se) catalysts (with alloyed and non-alloyed W(0))

The use of non-oxidized tungsten as co-catalyst in binary and ternary catalysts for fuel cells was also investigated. He et al. [95] used high-throughput combinatorial tools to investigate Pt-based binary alloy electrocatalysts for oxygen reduction. Based on the ORR activity and tolerance to chemical corrosion, the base metals were classified into four categories: (*i*) highly corrosive and highly active (Fe,Co,V,Mn); (*ii*) corrosive and highly active (Zn,Cu,Mo,Ni); (*iii*) stable but less active (Zr,Cr,Ta); and (*iv*) stable and active (W,Ti). Category (*iv*) elements were the most interesting, displaying both enhanced catalytic activity over pure platinum (up to 4 times) and chemical stability under testing conditions. Although their enhancement in ORR activity was lower than that of Pt-alloy containing category (*i*) and (*ii*) elements, PtTi and PtW alloys displayed strong corrosion resistance, which is highly necessary to prevent contamination of the membrane in fuel cells. In parallel to alloy electrocatalyst combinatorial discovery, they studied and developed synthesis technologies (core–shell and reverse microemulsion) to engineer alloy particles in the nanoscale. Though it has been demonstrated that the core–shell method is very successful in preparing single-metal and alloy nanoparticles, some limitations are evident. One example was the synthesis of PtW alloys. W is very amorphous after being reduced to metallic state and tends to deposit on the carbon surface, resulting is a secondary phase of either W or WO_3 that cannot be eliminated. To overcome this problem, a different synthesis technique is required. So, PtW nanoalloys were prepared using the reverse microemulsion

method. First, $W(OH)_x$ nanoparticles were prepared by hydrolyzing tungsten alkoxide. A platinum salt and reducing agent were then added to the microemulsion. The reduction reaction resulted in $Pt/W(OH)_x$ nanoparticles. Finally, the nanoparticles were loaded to the carbon surface, and heat-treated in hydrogen-containing atmosphere at 500–900 °C. Temperatures as high as 900 °C are required to form a pure PtW phase. Due to the high heat-treating temperature, particle agglomeration was expected, and very large particles (up to 20 nm) were formed. Below 900 °C, a secondary phase of metallic tungsten coexisted with the dominant PtW alloy phase. Even with a secondary W phase, the catalyst displayed a 2-times higher relative mass-specific activity as compared to Pt/C.

He and Xiong [96,97] synthesized carbon supported PtW alloy nanoparticles by thermal decomposition of carbonyl complexes at elevated temperatures. The structure of PtW alloy nanoparticles depends on the atomic ratio between Pt and W. Phase segregation was observed for high tungsten concentrations. Alloys with W concentrations up to 65 at% maintained the fcc type structure. Increasing W concentrations beyond 65% led to phase segregation as evidenced by the appearance of the α-W phase (bcc structure) in addition to the PtW alloy. The PtW/C alloy nanoparticles prepared by this route showed significantly higher ORR activity than Pt/C in an acidic electrolyte. The histogram of the relative mass specific activity at 0.8 V vs. Pt at% for the PtW alloys is shown in Fig. 7 from ref. 94. The maximum mass specific activity of PtW alloys was observed for 39 at% Pt, where ~3.4 time enhancement in catalytic activity was achieved. They also investigated the effect of annealing temperature on the relative mass specific activity of PtW (52:48). A maximum activity was found for an annealing temperature of 700 °C. Two factors may contribute to this phenomenon. First, the formation of a PtW alloy or increase of alloying extent with annealing temperature could increase the electrocatalytic activity. The mechanisms for catalytic enhancement of platinum alloys have been studied extensively and various possible reasons have been proposed including the role of alloy d-band center, modification of platinum d-band vacancy, Pt–Pt interatomic distance, the effect of alloy facets, the surface roughening due to leaching out of non-precious elements, and improved wettability of these alloys. Second, rapid particle growth resulted from high temperature annealing resulting in significant loss of electrochemical surface area and hence decreases of the catalytic activity. The interplay of particle size and alloying effect leads to the typical volcano type plot for PtW alloys.

Wang et al. [98] investigated the MOR activity of Pt-Ru-W/C and Pt-Ru/C catalysts, prepared by a thermal reduction method. Relative to the reflections in Pt alone and Pt-Ru, the XRD reflexions of Pt-Ru-W shifted slightly to higher 2θ values, indicating the formation of a ternary fcc PtRuW alloy. The MOR activity Pt-Ru-W/C was much higher than that of Pt-Ru/C.

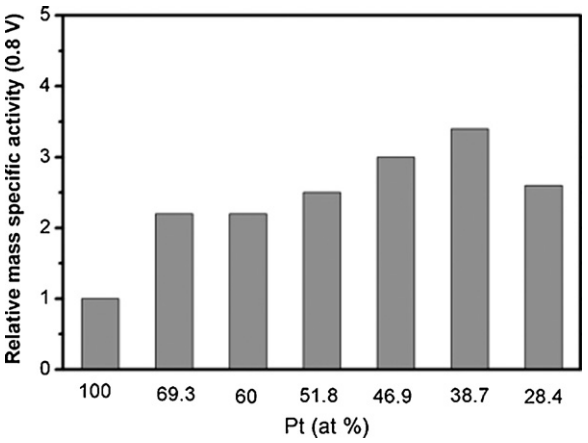

Fig. 7. Relationship between relative mass specific activity and Pt concentration in PtW alloys. Reproduced from Ref. [96], copyright 2006, with permission from Elsevier.

The group of Uchida investigated the activity of a ternary Pt-Ru-W catalyst for methanol [99] and ethanol [100] oxidation. They compared the MOR and EOR activities of Pt-Ru-W (65:20:15) with that of Pt-W (85:15) and of Pt-Ru alloys. The XRD pattern of Pt-W revealed the presence of the $\gamma(Pt_2W)$ phase. The XRD pattern of Pt-Ru-W, besides the peaks of the Pt_2W rhombic structure, showed the presence of the peaks belonging to hcp Ru structure. The diffraction peak intensity of the former was greater than that of the latter, indicating a Ru-dissolved Pt_2W structure. All the alloys exhibited catalytic activity higher than Pt. Compared to the binary alloys, higher current densities and a noticeable cathodic shift in the onset potential for both methanol and ethanol oxidation were observed at the Pt-Ru-W electrode. The onset potentials for the MOR matched well the anodic peak potentials recorded in the base electrolyte (H_2SO_4), i.e., 0.15 V versus Ag/AgCl for Pt-Ru-W and 0.35 V versus Ag/AgCl for Pt-W and Pt-Ru electrodes. From these findings, it was postulated that the background peak current generates oxide species necessary to complete the alcohol oxidation to CO_2. Pt-Ru-W electrode facilitates the generation of $M\text{-}OH_{ad}$ more than Pt-Ru or Pt-W. It is likely that the Ru-dissolved in the Pt_2W phase easily brings about the W/WO_x reaction rather than Pt_2W alloy.

Ru-Se-based catalysts (e.g., Ru-Se, Ru-Se-Mo, and Ru-Se-Rh) are promising materials as platinum-alternative cathode catalysts for DMFCs, presenting higher ORR activity than Ru alone and high methanol tolerance. However, their ORR activity is lower than that of Pt under fuel cell conditions. So, a further improvement in their activity is required. Cheng et al. [101,102] prepared modified ruthenium-selenium catalysts through the addition of tungsten. The novel catalysts were produced by decarbonylation of ruthenium and tungsten carbonyls in the presence of selenium and carbon powders, followed by annealing under hydrogen at 360 °C. In general, the Ru-Se-W catalysts presented smaller particle sizes than Ru-Se alone, indicating a decreased catalyst agglomeration due to the presence of tungsten. The increased surface area of the catalyst may be also due to physical modifications of the catalytically active Ru surface components by tungsten, e.g., via a corrosion effect. The XRD patterns of the carbon-supported $RuSe_{0.20}W_{0.14}$ material consisted of the crystalline hexagonal ruthenium and cubic tungsten phases. No distinctive Se phases were observed, most likely due to the overlap between the peaks of Ru and Se. The addition of tungsten led to a higher ORR activity, giving current densities up to 30% greater and cell power densities up to 25% greater than those obtained with Ru-Se alone. The $RuSe_{0.20}W_{0.29}$ catalyst showed the best DMFC performance with a maximum power density of 40 mW cm^{-2}. The cell performance improved with increasing tungsten content from 14 to 29 at%. A further increase to 58 at% leads to lower performance. The improved catalyst activity in the presence of tungsten was ascribed to different effects: (a) *Co-catalytic effect*. Tungsten addition leads to higher exchange current densities and lower activation energies for oxygen reduction, compared to the absence of tungsten, suggesting a co-catalytic effect of tungsten; (b) *Chemical effects*. The addition of tungsten has a stabilizing effect on Se. This has a beneficial influence on the oxygen adsorption and the electron transfer between reactants and the catalyst active sites because Se plays an active role in enhancing electron transfer and oxygen adsorption; (c) *Structural effects*. The presence of a crystalline tungsten phase has a beneficial influence on the catalyst activity towards oxygen reduction because the crystal faces of tungsten, e.g., the W(1 1 0) crystal face, are considered favorable sites for the chemisorptions of oxygen. The metal states of W and Ru in turn facilitates adsorption and activation of O_2 during electrocatalysis. The enlarged surface areas for the

Ru-Se-W catalysts, compared to Ru-Se alone, provide more active sites for oxygen reduction. On the other hand, tungsten alone has a lower activity than ruthenium. At a high ratio of tungsten to ruthenium, more surface areas are blocked by tungsten, which prevents oxygen accessing to the higher active ruthenium sites, leading to a lower overall performance. Moreover, it was found that the tungsten addition has an adverse effect on the methanol tolerance but the penalty seems not severe.

Recently, Sarkar et al. [103] synthesized carbon supported $Pd_{100-x}W_x$ ($0 \le x \le 30$) alloy electrocatalysts by simultaneous thermal decomposition of palladium acetylacetonate and tungsten carbonyl in the presence of Vulcan XC-72R carbon, followed by annealing up to 800 °C in H_2. Characterization of the Pd-W samples indicated the formation of single phase fcc solid solutions for $0 \le x \le 20$. The particle size was *ca.* 10 nm, with a slightly broader size distribution. Electrochemical measurements revealed that the alloying of Pd with W enhances the catalytic activity for the ORR as well as the stability of the electrocatalyst compared to the unalloyed Pd. The composition $Pd_{95}W_5$ exhibited the maximum ORR activity in the Pd-W system, with the mass activity comparable to that of Pt. The Pd-W catalysts showed higher tolerance to methanol electro-oxidation compared to that of Pt, which may offer important advantages in employing these electrocatalysts for ORR in DMFCs.

3.4. Pt-polyoxometallates and Pt-heteropolyacids

Polyoxometallates are large crystalline discrete molecular structures composed of metal cations bridged by oxide anions, providing high electron affinity [104]. The most investigated of all structural types are the Keggin heteropolyanions of formula $[X^{n+}M_{12}O_{40}]^{(8-n)-}$, when M = W(VI) or Mo(VI). The heteroatom, X^{n+}, can be a nonmetal, semimetal and/or even metal. X^{n+} is, for example, phosphorus in $[PW_{12}O_{40}]^{3-}$, a classical anion of the Keggin structural type. Heteropolyacids (HPAs) are a subset of the polyoxometalates. HPAs are very strong Bronsted acids, well known proton conductors, and they also exhibit fast reversible multielectron redox behavior under mild conditions.

The modification of Pt nanoparticles by Keggin-type polyoxometallates or heteropolyacids as potential activating agents for the oxygen reduction was extensively investigated by the group of Kulesza [105–108]. Kulesza et al. [105] investigated the ability of $[PW_{12}O_{40}]^{3-}$ to form stable anionic monolayers on solid surfaces. Three-dimensional assemblies on electrode surfaces were grown using the layer-by-layer method involving repeated alternate treatments in the solution of $[PW_{12}O_{40}]^{3-}$ (or in the colloidal suspension of polyoxometallate-protected Pt-nanoparticles) and in the solution of monomer (e.g., anilinium) cations. In the resulting structured (organic–inorganic) films, the layers of negatively charged polyoxometallate, or polyoxometallate-protected Pt-nanoparticles, interacted electrostatically with the ultra-thin layers of positively charged polyaniline. The modification of Pt nanoparticles by adsorbing monolayers of phosphododecatungstate tends to activate them towards efficient ORR in acid medium. Wlodarczyk et al. [106] modified platinum nanoparticles, firstly deposited on glassy carbon, with ultra-thin films of polyoxometallates through their spontaneous adsorption on solid surfaces. $H_3SiW_{12}O_{40}$, $H_3SiMo_{12}O_{40}$, $H_3PW_{12}O_{40}$ and $H_3PMo_{12}O_{40}$ were considered as potential activating agents. By rotating disk electrode (RDE) measurements in H_2SO_4 solution at 25 °C, statistically higher (in comparison to bare Pt) electrocatalytic currents for the ORR were observed upon introduction of monolayers of heteropolyanions. Among the polyoxometallates considered, the system modified with $H_3PW_{12}O_{40}$ (PWA) was the most effective. Although the possibility of structural changes cannot be excluded, the synergistic effect originated presumably from the bifunctional activity of the electrocatalyst. While Pt retained its usual reactivity towards the oxygen reduction, $H_3PW_{12}O_{40}$ could act as both effective mediator (e.g., for the reduction of the hydrogen peroxide intermediate) and the source of mobile protons at the electrocatalytic interface. In a next work, Wlodarczyk et al. [107] used Nafion®-stabilized inks of carbon supported Pt nanoparticles to produce electrocatalytic films on glassy carbon. The catalysts were modified with PWA. RDE measurements indicated that the reduction of oxygen at the PWA-modified electrode proceeded at *ca.* 30–60 mV more positive potential (depending on the PWA content), and the system was characterized by a higher rate of heterogeneous electron transfer, when compared to the PWA-free electrocatalyst. Gas diffusion electrodes with Pt/C supported on carbon paper were also tested: the exchange current density and the total resistance contribution to polarization components, obtained from galvanostatic polarization curves, were clearly higher and lower, respectively, for the PWA-modified ink relative to the unmodified system. The results demonstrate that addition of PWA (together with Nafion®) enhances the ORR activity of platinum. Chojak et al. [108] characterized surfaces of bulk platinum and unsupported Pt nanoparticles, modified and stabilized with $H_3PMo_{12}O_{40}$ (PMA) and $H_3PW_{12}O_{40}$. The presence of the polyoxometallate monolayer on platinum resulted in the partial suppression of the interfacial formation of PtOH/PtO oxides. Both molybdates and tungstates seem to interact with Pt surface via their corner oxygen atoms. The existence of spacious, largely hydrated, polyoxometallate monolayers on platinum did not block access of oxygen to the catalytic Pt sites. The modification of Pt with PWA (but not with PMA) resulted in the ORR enhancement.

The effect of polyoxometallates on the activity for methanol oxidation of Pt and Pt-Ru catalysts was also investigated. Nakajima and Honma [109] reported the synthesis of platinum-coordinated polyoxometalates and their MOR activity. Pt was coordinated stoichiometrically in the lacunary site of Keggin-type polyanion by the reaction of tetrabutylammonium α-undecatungstosilicate and H_2PtCl_6. This catalyst showed high methanol oxidation current despite the low Pt/polyoxometallate ratio (4.8 wt%). Chojak et al. [110] prepared hybrid films composed of $[PW_{12}O_{40}]^{3-}$ linked oxoruthenium-coated Pt nanoparticles using the layer-by-layer method. By repeated alternate treatments in a solution of $[PW_{12}O_{40}]^{3-}$ and in a colloidal suspension of oxoruthenium-protected Pt nanoparticles, the film thickness can be increased systematically to form stable three-dimensional assemblies on carbon electrodes. The addition of phosphotungstate to oxoruthenium-coated Pt nanoparticles enhanced the MOR activity in acid solution of this catalyst. The catalytic enhancement may be due to the synergistic effect between Pt-Ru and $[PW_{12}O_{40}]^{3-}$. Tungstate units may provide additional –OH groups or radicals capable of facilitating oxidation of CO_{ads} on Pt. Alternatively, introduction of $[PW_{12}O_{40}]^{3-}$ may induce morphological differences and lead to better catalyst utilization. Ferrell et al. [111] tested a single DMFC incorporating PWA and PMA in the anode Pt/C catalyst layer. Both the cells with Pt/C-PWA and Pt/C-PMA showed higher performance than that with Pt/C. From the impedance model they found that the incorporation of HPAs into the catalyst layer resulted in a reduction in the resistance to charge transfer. Maiyalagan [112] prepared silicotungstic acid (SiWA) stabilized Pt-Ru nanoparticles supported on functionalized carbon nanofibers by a microwave-assisted polyol process. The MOR activity of the composite (20% Pt-Ru-SiWA/CNF) catalyst was higher than that of 20% Pt-Ru/C and 20% Pt-Ru-SiWA/C. The enhancements in activity and stability over Pt-Ru-SiWA/CNF catalyst was attributed to highly dispersed Pt-Ru nanoparticles on the CNF and enhanced methanol oxidation due to the presence of SiWA, facilitating the oxidative removal of poisoning species on Pt.

3.5. K_2WO_4 in MCFCs

Molten carbonate fuel cells are high-temperature fuel cells that use an electrolyte composed of a molten carbonate salt mixture suspended in a porous, chemically inert ceramic matrix of beta-alumina. Because of the high operation temperature (650 °C) and the presence of corrosive molten alkaline carbonate degradation of the components can easily occur. Greater cell life is one of the most important targets for MCFC to be brought into actual application. A key point in the development of electrode materials for MCFCs is improvement in both the power output and the stability. Porous nickel is commonly used as the anode for MCFCs; its performance is relatively satisfactory, but the sintering and creep resistance should be increased. Ni-Cr, Ni-Co or Ni-Cu alloys are considered as possible anode materials. Another key point is the amount of electrolyte in the cell. It is well known that one of the major causes of the deterioration of MCFCs is electrolyte depletion. Indeed, the cell performance depends greatly on the amount of electrolyte in the cell. Lithium aluminate, the state-of-the-art matrix support material, plays a role of maintaining the amount of electrolyte in the matrix at an appropriate level. The phase transformation and particle growth of $LiAlO_2$ particles, observed after a long period of cell operation, is a serious problem and must be overcome in order to attain more than 40,000 h of MCFC life. These effects cause pore coarsening of the porous matrix substrate and reduce the capillary force required to retain the electrolyte in its pores [113].

To increase the stability of the anode, Yabe et al. [114] modified the surface of a porous nickel electrode by electrodeposition of tungsten from a LiC1–KC1 eutectic melt containing K_2WO_4. Polarization measurements showed that the performance of an MCFC anode modified by tungsten is superior to that of bare porous nickel. These anodes showed greater durability and enhanced resistance to corrosion. In another experiment, they found that the porous nickel electrode itself gives excellent performance as an MCFC anode when K_2WO_4 is added to the electrolyte. This behaviour is considered to be the result of *in situ* modification of the electrode surface. Then, Xie et al. [115] investigated the mechanism of *in situ* surface modification of molten carbonate fuel cell anode by the addition of tungstate ion to the electrolyte. They concluded that tungsten dissolves in molten carbonate in several valence states from +2 to +6 with a potential dependency, the reduction of tungstate is quite irreversible, and with addition of tungstate, the performance of an MCFC anode can be improved through indirect oxidation of hydrogen. Moreover, they observed that deposition of tungsten metal on the surface of a porous nickel anode also improves the mechanical properties of the anode.

Terada et al. [116] studied of the mechanism of particle growth and phase transformation of $LiAlO_2$, as well as the effect of additives for inhibiting particle growth. They found that potassium tungstate inhibits the particle growth of the lithium aluminate containing β-phase. In a next paper, the same authors [117] conducted endurance tests were conducted in a 100-cm^2 single cell for more than 10,000 h in order to verify the effect of K_2WO_4 added to the matrix on anode sintering, separator corrosion, cathode solubility, and matrix stability. A Ni or Ni-Al anode and a NiO cathode were used in the single cells. The composition of the carbonate was 62 mol% Li_2CO_3, 38 mol% K_2CO_3 with the addition of 1.4 wt% K_2WO_4. Porous nickel anodes without K_2WO_4 additions showed a substantial loss of pore volume. By contrast, the loss of pore volume in porous nickel anodes with K_2WO_4 additions was substantially decreased; there was an initial drop in pore volume over 400 h but little change thereafter (~80% of initial value after 1000 h). This effect was ascribed to reduction of tungstate ion to produce tungsten metal on the porous nickel electrode under H_2. The results of corrosion studies using stainless-steel 316L test pieces under cathode conditions indicated that K_2WO_4 addition has some effect on the corrosiveness of the melt and minimum corrosion was attained at 1.4 wt% addition of K_2WO_4. In the absence of K_2WO_4, the oxide scale at the central part of the test piece fell off and can be considered to penetrate the substrate by corrosion. When 1.4 wt% K_2WO_4 was added to the electrolyte, a thick film was formed and was considered to decrease the rate of corrosion. The solubility of a NiO cathode is slightly lowered by the presence of the tungstate salt in a low CO_2 environment, but is not affected under normal operational conditions. An increase in the α-$LiAlO_2$ phase and decreases in the β-$LiAlO_2$ and γ-$LiAlO_2$ phases was observed in the absence of tungstate. The corresponding changes in phase transformation are small in the presence of tungstate. In particular, there is a slight increase in the γ-$LiAlO_2$ phase.

Electron probe micro-analysis (EPMA) was used to determine the distribution of tungsten concentration across the anode and the electrolyte matrix after 10,000 h cell operation when using a pure Ni anode. The concentration of tungsten at the anode is higher than that at the matrix. This means that WO_4^{2-} converts into other insoluble compounds at the anode as a sink and the diffusion of WO_4^{2-} ions from the matrix to the anode occurs. Such compounds of tungsten are supposed to be formed through reduction of WO_4^{2-} ions by dissolved hydrogen in the electrolyte. These compounds precipitate around the anode particles and retard the sintering of Ni anode. The cell was operated for more than 10,000 h without electrolyte replenishment. After 13,000 h, the cell performance drastically dropped because a short-circuit occurred abruptly by NiO dissolution-precipitation. The degradation rate of voltage up to 13,000 h was less than 0.3%/1000 h. Thus, it is confirmed that the addition of K_2WO_4 to the electrolyte of an MCFC is effective for a long life.

4. Tungsten oxides and carbides as carbon-alternative catalyst supports

Catalysts supported on high surface area carbons are widely used in low-temperature fuel cells. However, the corrosion of carbonaceous catalyst-support materials such as carbon black has been recognized as one of the causes of performance degradation of low-temperature fuel cells, in particular under repeated start-stop cycles or high-potential conditions. To improve the stability of the carbon support, materials with a higher graphitic character such as carbon nanotubes and carbon nanofibers have been tested in fuel cell conditions. These nanostructured carbons show a several-fold lower intrinsic corrosion rate, however, do not prevent carbon oxidation, but rather simply decrease the rate. Due their high stability in fuel cell environment, ceramic materials such as WO_3 and W_xC have been investigated as carbon-substitute supports for fuel cell catalysts. The increasing interest on the use of these tungsten-based materials as catalyst supports is also due to the possibility of a synergistic effect between the supported metal catalyst and the ceramic support. Thus, tungsten oxides and carbides have been tested as carbon-alternative supports for fuel cells.

4.1. WO_3

It has been previously shown that tungsten oxides exhibit considerable proton transfer because of the formation of tungsten trioxide hydrates, which is an attractive property for fuel cell catalyst supports. WO_3 has been shown to be more thermally stable under electrochemical oxidation conditions than Vulcan XC-72R carbon [118]. Recently, some papers have been addressed to the use of WO_3 microspheres and mesoporous or nanostructured tung-

sten oxides as carbon-alternative supports for fuel cell catalysts. These materials possess interesting properties as higher stability and higher surface area than the conventional WO_3. Ganesan and Lee [119] and Cui et al. [120], in microsphere and mesoporous form, respectively, and Rajeswari et al. [121] and Maiyalagan and Wiswanathan [122], in nanorod form, tested WO_3 as a carbon-substitute support for DMFC catalysts. Ganesan and Lee [119] prepared WO_3 microspheres of 2–4 μm size by controlled oxidation of W_2C microspheres. Platinum particles were supported on WO_3 microspheres and carbon microspheres by the borohydride reduction method (BM), consisting in the deposition of H_2PtCl_6 on the substrate, followed by reduction with $NaBH_4$. The average crystallite size was 6.5 and 15 nm for Pt and WO_3, respectively. The pore-size distribution of WO_3 showed a large number of pores of around 45 nm. The large pore-size was attributed to the inter-particle spaces between WO_3 nanoparticles. The BET surface area of the WO_3 microspheres was about 18 $m^2\,g^{-1}$. WO_3 supported Pt displayed higher MOR activity than a commercial Pt-Ru/C by a factor of 1.9 (per mass of Pt) even without Ru. The onset potential and peak potential of methanol oxidation on Pt/WO_3 were shifted by 100 and 50 mV more negative than Pt-Ru/C, probably due to its better CO tolerance. The stability of the Pt/WO_3-microsphere catalyst was tested by repeating electrochemical cycles in a H_2SO_4/CH_3OH solution. The specific activity increased initially, but stabilized after about 15 cycles. Once a steady-state is established, there was no sign of deactivation during 100 consecutive reaction cycles.

Cui et al. [120] synthesized mesoporous WO_3 with ordered pore structure by a template replicating route. Pt was deposited on mesoporous WO_3 by the BM. The BET surface area of the mesoporous WO_3 was 86 $m^2\,g^{-1}$, and the average crystallite size of Pt was about 6.5 nm. Pt/WO_3 showed high MOR activity and good electrochemical stability. The MOR activity of 20 wt% Pt/WO_3 was significantly higher than that of a commercial 20 wt% Pt/C. The enhanced MOR activity on Pt/WO_3 was ascribed to the enhanced catalytic effect and the mesoporous structure of WO_3 support.

Recently, one-dimensional (1D) nanorods have attracted remarkable attention owing to their unique properties and potential for various novel applications [123]. Nanorods have large specific surface areas, so WO_3 in a nanorod form could be an efficient support for fuel cell catalysts. Rajeswari et al. [121] synthesized WO_3 nanorods (WO_{3nano}) by pyrolysis of tetrabutylammonium decatungstate, $((C_4H_9)^4N)^4W_{10}O_{32}$, at 450 °C. In the precursor compound, inorganic metal oxide clusters ($W_{10}O_{32}{}^{4-}$) are charge balanced with the surfactant group tetrabutylammonium bromide (TBABr). TBABr restricts the irregular arrangement of the metal oxide clusters by providing a steric environment around them. This leads to the formation of 1D array of metal oxide clusters. The dimensions of the nanorods varied in the ranges of 130–480 nm and 18–56 nm of length and width, respectively. Pt nanoparticles were supported on WO_3 (20 wt% Pt) by the wet impregnation method. The size of the Pt nanoparticles was is in the range of 4–6 nm. The electrochemical stability of WO_{3nano} and bulk WO_3 (WO_{3bulk}) was studied in 1 M H_2SO_4 by repetitive potential cycling (RPC) between −0.2 and 1.0 V. For the WO_{3nano} almost no activity variation was observed even after several cycles indicating its stability in H_2SO_4. For the WO_{3bulk}, instead, the peak current was observed to decrease, showing a poor stability in acid medium. The MOR activities of Pt loaded WO_{3nano}, a commercial 20 wt% PtRu/C and Pt loaded on bulk WO_3, were in the following order: Pt/WO_{3nano} >PtRu/C > Pt/WO_{3bulk}. The activity of Pt/WO_{3nano} was approximately six times higher than that of the Pt/WO_{3bulk}, clearly indicating that the nanostructure of the catalytic support plays an essential role. Maiyalagan and Wiswanathan [122] synthesized WO_3 nanorods infiltrating a PWA solution into an alumina membrane as a template, then platinum nanoparticles were supported on the nanorods by an impregnation method. The diameter of the nanorods was around 200 nm. The size of the Pt nanoparticles was in the range of 3–4 nm. WO_3 stability tests, carried out by RPC in 1 M H_2SO_4, showed that WO_3 nanorods have higher stability compared with bulk WO_3. Pt/WO_3 nanorods exhibited higher MOR activity than Pt/C by a factor of two. Platinum supported on such nanorods was stable over several cycles in an electrochemical environment.

4.2. WC and W_2C

Recently, the use of tungsten carbides as carbon-alternative support for low-temperature fuel cell catalysts has received considerable attention. As electrocatalysts, they are highly resistant to CO poisoning and stable in acidic and basic solutions, but their electrocatalytic activity for methanol oxidation is low. However, as previously reported, their activity could be improved by adding a small amount of platinum to tungsten carbides. Analogously, the presence of tungsten carbide promotes the electrochemical activity for oxygen reduction of platinum. Zhang et al. [124] compared the electrochemical activity and stability in PEMFC environment of W_xC supported Pt with that of carbon supported Pt. The tungsten carbide support was prepared through the carbonization method using C and H_2WO_4 as precursors. Pt was deposited on the tungsten carbide and Vulcan XC-72 by the formaldehyde reduction method. The Pt loading of the catalysts was 10 wt%. XRD patterns showed the diffraction peaks of Pt, WC, W_2C, and $W_2C_{0.85}$. The initial electrochemically active surface area (EASs) of Pt/C was higher than that of Pt/W_xC, due to the higher surface area of Vulcan XC-72 than that of tungsten carbide. The EAS loss of the Pt/W_xC during the stability test in H_2SO_4 at various potentials was much lower than that of Pt/C. Before stability test, the PEMFC with Pt/C better performed than that with Pt/W_xC. After stability test, instead, the cell with Pt/W_xC showed enhanced performance than the cell with Pt/C, indicative of a high oxidation resistance of the W_xC support. Jeon et al. [125] prepared a 20 wt% Pt/WC by an impregnation method and compared its MOR activity with that of a commercial 20 wt% Pt/C. Commercial WC powder was used as a support. Average particle sizes of Pt in Pt/WC and Pt/C were 7.5 and 2.9 nm, respectively. The higher Pt particle size in Pt/WC was ascribed to the larger density of WC. EASs calculated from CO stripping were 4.42 and 6.30 $m^2\,g^{-1}$ for Pt/WC and Pt/C, respectively. CO electro-oxidation peak potential shifted from 0.80 V in Pt/C to 0.68 V in Pt/WC. The improved CO oxidation activity originated from formation of OH by water discharge on the WC surface. The mass activity for methanol oxidation of Pt/WC was lower than that of Pt/C. The specific activity of Pt/WC, instead, was higher than that of Pt/C. Chhina et al. compared the stability of Pt supported on commercial WC (BET = 1.6 $m^2\,g^{-1}$) with that of a homemade Pt/C [126] and a commercial Pt/C [127]. Comparisons of activity change with cumulative oxidation cycles were made between C and WC supports with comparable loadings of catalyst by weight, solid volume, and powder volume. In all cases, Pt/WC was more thermally and electrochemically stable than Pt/C. The electrochemical activity of the Pt/WC remained nearly constant over 100 accelerated oxidation cycles, while the activity of Pt/C was almost completely lost after only approximately 20 oxidation cycles. The high stability of Pt/WC was ascribed to the surface oxidation of W during the first scan, changing the structure of the catalysts from Pt supported on WC to Pt supported on a WO_x shell encapsulating a WC core. Since tungsten oxide exhibits fairly high electrochemical stability, its formation is less deleterious to fuel cell performance than the oxidation of a carbon support, which leads to irreversible platinum detachment and corresponding complete activity loss. However, the initial activity of Pt/WC was much lower than that of Pt/C at comparable volu-

metric catalyst loadings, indicating that higher surface area WC supports and better platinum dispersion techniques are required to enhance the catalytic activity. To prepare high surface area WC, Chhina et al. [127] synthesized WC using high surface area carbon as a template upon which tungsten was dispersed by three different routes: aqueous tungstate dispersion on carbon, an incipient wetness technique to disperse tungstate on carbon, and DC magnetron sputtering of tungsten on carbon. Only DC magnetron sputtering of W onto C proved to be a promising technique for high surface area WC synthesis, leading to porous agglomerates that were not as dense as those obtained by either of the other two techniques.

Hara et al. [128] prepared a 10 wt% Pt/WC by a wet impregnation method. A WC (surface area of 25.6 $m^2\,g^{-1}$) support, obtained by carburization of W_2N, which was synthesized from WO_3, was used. Pt particles were fairly aggregate with around 20 nm in size, due to the low surface area of WC. The mass activity for the HOR of Pt/WC was lower than that of a commercial Pt/C, due to its lower EAS. The specific activity of Pt/WC, instead, was higher than that of Pt/C. The same research group [129] prepared new WCs with high surface area by the carburizing of W_2N and WS_2 precursors, which were prepared from starting materials other than WO_3, such as $W(CO)_6$ and WCl_6 and the like. In particular, the BET surface areas of WCs derived from $W(CO)_6$/S and $(NH_4)_2WS_4$ were around 80 $m^2\,g^{-1}$, the highest value among α-WCs reported. This is probably due to a unique structural change forming small crystalline WC particles with a plate-like structure in the carburization of WS_2 and W_2N. As a result, the mass activity for the HOR of the Pt/WC catalyst was superior to that of Pt/C. The interaction of Pt with WC leads to a remarkable improvement in terms of activity, due to a strong synergistic effect. They postulated that Pt play the role at accelerating the process of the dissociative adsorption of H_2, which is the rate-determining step for the HOR on WC, and WC could take over the rest of steps in the process of the hydrogen electro-oxidation.

As in the case of WO_3, some papers have been addressed to the use of tungsten carbide microspheres or mesoporous tungsten carbide as fuel cell catalyst supports. Ganesan and Lee [130] synthesized W_2C microspheres (W_2CMS) by heating mixtures of resorcinol-formaldehyde and ammonium metatungstate (AMT). XRD analysis indicated W_2C as the major phase, and WC and WC_{1-x} as minor phases. The BET surface area of the W_2CMS was about 176 $m^2\,g^{-1}$ (compared to 635 $m^2\,g^{-1}$ for carbon microspheres (CMS)). Pt and Pt-Ru particles were supported on W_2CMS and on CMS, respectively, by the BM. The crystallite sizes were 6 and 14 nm for 7.5 and 15 wt% Pt/W_2CMS, respectively, and 14 nm for 20 wt% Pt-Ru/CMS. The electrochemical surface area of Pt/W_2CMS was several times higher than those of Pt-Ru/CMS and a commercial 20 wt% Pt-Ru/C catalyst. The MOR activity of the Pt/W_2CMS catalysts was higher than that of Pt-Ru/CMS and PtRu/C catalysts. The mass activity of 7.5 wt% Pt/W_2CMS was higher by factors of 2.6 and 2.4 than those of Pt-Ru/CMS and PtRu/C, respectively. These results clearly showed that Pt/W_2CMS provides much better utilization of platinum than Pt-Ru/CMS and PtRu/C and that ruthenium could be entirely replaced. According to the authors, there are several reasons why Pt/W_2CMS better performs than Pt-Ru/C. The first is the ability of W_2C to stabilize the high dispersion of platinum relative to carbon supports as discussed above. Second, in the presence of platinum, W_2C is active in the electrochemical methanol oxidation and water decomposition. The formation of hydroxy groups from water activation is essential for the removal of metal-poisoning CO from the surface. This is the main role played by ruthenium in conventional Pt-Ru catalysts and this role can be played by W_2C. Finally, W_2C showed high CO resistance. The CO desorption temperature for pure platinum is 187 °C. It decreases to 147 °C, when the platinum is supported on W_2C. This feature would decrease the poisoning of the catalyst surface by CO and increase the MOR activity. The stability of Pt/W_2CMS was tested by RPC in a H_2SO_4/CH_3OH solution. The specific activity increased initially, but stabilized after around 30 cycles, without signs of deactivation during 100 consecutive reaction cycles. In a similar work, Wang et al. [131] synthesized tungsten carbide microspheres (WCMS) with uniform particle size and high surface area (256 $m^2\,g^{-1}$) by using a hydrothermal method. Pt nanoparticles were uniformly distributed on these support materials through the IMH method. The as-prepared Pt/WCMS catalyst showed superior performance to that of Pt/CMS and Pt/C catalysts in terms of ORR onset potential and mass activity. The enhanced performance of Pt/WCMS for the ORR could be attributed to its higher electrochemical surface area, as well as to the synergistic effect between Pt and WC. Ganesan et al. [132], Ham et al. [133] and Wang et al. [134] tested mesoporous tungsten carbides as Pt supports. Ganesan et al. [132] synthesized mesoporous tungsten carbides by polycondensation of resorcinol-formaldehyde in the presence of AMT, followed by heat treatment at 900 °C. They prepared two-types of WC powders by controlling the amount of mesopores. The difference in the preparation methods was the presence or absence of a surfactant (cetyltrimethylammonium bromide, CTABr) during the polycondensation step. The preparation with CTABr gave WC with ample mesoporosity (denoted as meso-WC) whereas that without CTABr yielded WC nanoparticles with a small pore volume (denoted as part-WC). Average pore sizes and BET surface areas of meso-WC and part-WC were similar, 4.6 nm and 95 $m^2\,g^{-1}$ for part-WC, and 4.3 nm and 76 $m^2\,g^{-1}$ for meso-WC, respectively. The most significant difference between two samples was the pore volume, 0.086 $cm^3\,g^{-1}$ for the part-WC and 0.24 $cm^3\,g^{-1}$ for the meso-WC. The XRD pattern of meso-WC sample showed the presence of WC as the major phase, and minor amounts of W_2C and WC_{1-x}. WC particle size was *ca.* 20 nm. Pt particles were deposited on these WC materials by the BM. The average Pt particle size was *ca.* 2 nm for 3.5 wt% Pt and *ca.* 6 nm for 7.5 wt% Pt both on part-WC and meso-WC. Pt supported on these materials showed higher MOR activity than a commercial PtRu/C catalyst by a factor of six (per mass of Pt) even without Ru. The mesoporosity and phase of WC appear important as Pt/meso-WC better performed than Pt/W_2C-microsphere and Pt/part-WC. It is interesting to note that the two less active tungsten carbide catalysts possess higher surface areas than that of Pt/meso-WC, but they are mostly due to micropores. Thus, the facile mass transport of hydrated methanol to the reaction sites through the mesoporous structure seems to be crucial to obtain high electrocatalytic activities. Ham et al. [133] prepared a mesoporous tungsten carbide by using the same method of Ganesan et al. [132] previously described, then deposited Pt on the mesoporous WC by the BM (7.5 wt% Pt). The Pt/WC catalyst shows not only two times higher mass activity for hydrogen electro-oxidation, but also much improved resistance to CO poisoning than Pt/C. The high HOR activity was attributed to the active participation of WC in the electro-oxidation and the high CO tolerance to facile formation of surface hydroxyls on WC that could react with CO strongly adsorbed on Pt. It has to be remarked that in both these works using mesoporous carbon the Pt/WC weight ratio was <10 wt%. Very recently, Wang et al. [134] synthesized a nanochain-structured mesoporous tungsten carbide (*m*-NCWC) material with high specific surface area (113 $m^2\,g^{-1}$) by combining a surfactant assisted hydrothermal reaction and a thermal treatment process. The *m*-NCWC synthesized at the optimized conditions showed an interesting mesoporous nanochain-structure (lengths over ~200 nm to 2 μm and diameters from 50 to 100 nm). The W:C atomic ratio of nanochains was 0.9:1. Pt supported on *m*-NCTC carbon microspheres showed higher electroactivity and better resistance to CO poisoning than Pt/C.

The characteristics of tungsten oxides and carbides as catalyst supports are summarized in Table 1.

5. Tungsten-based proton conducting materials in composite membranes

5.1. Heteropolyacids (HPAs)

Heteropolyacids have been largely employed as catalysts in heterogeneous reactions due to their unique structural and chemical properties. There are three main commercially produced HPAs: 12-phosphotungstic acid (PWA), 12-phosphomolybdic acid (PMA), and 12-silicotungstic acid (SiWA). The basic structural unit of heteropolyacids is the Keggin anion $(PM_{12}O_{40})^{3-}$ (M = Mo or W) or $(SiW_{12}O_{40})^{4-}$ which consists of the central PO_4 or SiO_4 tetrahedron surrounded by twelve MO_6 octahedra. In the case of PWA, four types of oxygen atoms can be distinguished. The central oxygen atom belonging to the PO_4 tetrahedron is shared by the three tungsten atoms of the set. The edge-sharing oxygen atom will bridge two tungsten atoms of the same set. The corner-sharing oxygen atom bridge two tungsten atoms of different sets. The terminal oxygen atom is associated with a single tungsten atom. The bridging and terminal oxygen atoms are on the periphery of the structure and therefore are available to associate with protons or water molecules to form hydrates. Actually, they form channels which can contain up to 29 water molecules in at least four different hydrate phases (n = 29, 21, 13–14, 6). It is well known that the heteropolyacid hydrates lose water molecules even at room temperature and are transformed to lower hydrates. In the 29 hydrates only six water molecules occupy ordered sites and only these water molecules have a structural function. For other water molecules, there is little evidence of an ordered structure and it could be said that they have a statistical arrangement with numerous possible interactions within the available volume.

Table 1
Structural characteristics of supports and supported catalysts, and electrochemical activity and stability of Pt/WO_3 and Pt/W_xC catalysts.

Support	Structural characteristics of WO_3, W_xC and supported Pt	Electrochemical activity and stability of Pt/WO_3 and Pt/W_xC.	References
WO_3 microspheres	BET surface area WO_3 18 $m^2\ g^{-1}$ Large WO_3 pore-size Pt crystallite size 15 nm	Higher MOR activity of Pt/WO_3 than a commercial Pt-Ru/C. High stability	[119]
Mesoporous WO_3	BET surface area WO_3 86 $m^2\ g^{-1}$ Pt crystallite size 6.5 nm (20 wt% Pt)	Higher MOR activity of Pt/WO_3 than a commercial Pt/C	[120]
WO_3 nanorod	WO_3 nanorod in the ranges 130–480 nm length and 18–56 nm width. Pt particle size 4–6 nm (20 wt% Pt)	MOR activity order: Pt/WO_{3nano} > PtRu/C > Pt/WO_{3bulk} Stability Pt/WO_{3nano} > Pt/WO_{3bulk}	[121]
WO_3 nanorod	WO_3 nanorod diameter 200 nm. Higher stability of WO_{3nano} than WO_{3bulk} Pt particles size 3–4 nm	Higher MOR activity of Pt/WO_{3nano} than Pt/C High stability of Pt/WO_{3nano}	[122]
W_xC	W_xC mix of WC, W_2C, and $W_2C_{0.85}$	Before stability test, the PEMFC with Pt/C better than that with Pt/W_xC. After stability test, PEMFC with Pt/W_xC better than that with Pt/C Higher stability of Pt/W_xC than Pt/C.	[124]
Commercial WC	Low WC surface area Pt particle size 7.5 nm (20 wt% Pt)	Improved CO oxidation activity. Mass MOR activity of Pt/WC lower than that of Pt/C. Specific MOR activity of Pt/WC higher than that of Pt/C	[125]
Commercial WC	BET surface area 1.6 $m^2\ g^{-1}$	HOR activity of Pt/WC much lower than that of Pt/C Pt/WC more thermally and electrochemically stable than Pt/C	[126]
WC by carburization of W_2N from WO_3	BET surface area 25.6 $m^2\ g^{-1}$ Pt particle size 20 nm	Mass HOR activity of Pt/WC lower than that of Pt/C. Specific HOR activity of Pt/WC higher than that of Pt/C	[128]
WC by carburization of W_2N and WS_2 from $W(CO)_6$/S and $(NH_4)_2WS_4$	BET surface area 80 $m^2\ g^{-1}$	Mass HOR activity of Pt/WC higher than that of Pt/C	[129]
W_2C microspheres	BET surface area 176 $m^2\ g^{-1}$ Pt crystallite sizes 6 nm (7.5 wt% Pt) and 14 nm (15 wt% Pt)	High CO resistance. MOR activity of Pt/W_2CMS catalysts higher than that of Pt-Ru/CMS and PtRu/C catalysts High stability	[130]
WC microspheres	BET surface area 256 $m^2\ g^{-1}$	Higher ORR activity of Pt/WCMS than that of Pt/CMS and Pt/C	[131]
Mesoporous WC	BET surface area 95 $m^2\ g^{-1}$ Pore volume 0.24 $cm^3\ g^{-1}$ Pt particle size 2 nm (3.5 wt% Pt) and 6 nm (7.5 wt% Pt)	Higher MOR activity of Pt/WC than a commercial PtRu/C	[132]
Mesoporous WC	BET surface area 76 $m^2\ g^{-1}$ Pore volume 0.24 $cm^3\ g^{-1}$ Pt particle size 5.7 nm (7.5 wt% Pt)	High CO resistance. Mass HOR activity of Pt/WC higher than that of Pt/C	[133]
Mesoporous WC	BET surface area 113 $m^2\ g^{-1}$ Pt particle size 4 nm	Higher CO resistance and MOR activity of Pt/WC than Pt/C	[134]

An excellent review on the structure of HPA hydrates and the physicochemical properties of HPA-water system has recently done by Micek-Ilnicka [135].

This variety of interactions gives a possibility of forming different protonic species and hydrogen bonds of different strength. The consequence of this is one of the principal properties of these compounds – high protonic conductivity, 2×10^{-2} to 10^{-1} S cm^{-1} at room temperature – so that they belong to the group of superionic conductors [136]. Such high ionic conductivity together with the lower cost with respect to polymer membranes, make HPAs very attractive for fuel cells.

5.1.1. Early studies at CNR-ITAE, Messina, Italy

The first fuel cells with PWA as the electrolyte were realized at CNR ITAE, Messina, Italy [137–141]. Giordano et al. [137] realized a low-temperature H_2/O_2 fuel cell based on PWA as the electrolyte. Glass microfiber felt was utilized as electrolyte matrix. Pt/C catalysts were used as electrode materials. An output electrical power of 700 mW cm^{-2} was obtained at 25 °C and 1 atm. Cell performance was mainly determined by the high conductivity characteristics of the electrolyte and its promoting effect towards the ORR. Then, Staiti et al. [138] compared the performance of fuel cells fed with H_2/O_2 at room temperature utilizing two different PWA-based electrolyte layers. The fuel cell with a composite electrolyte layer formed of 30 wt% of silicon polymer and 70 wt% of PWA showed poor electrochemical performance. The main reason for this result was the high internal resistance of the cell. Furthermore, the silicon polymer utilized in the electrolytic layer degraded under the working conditions of the fuel cell. On the other hand, the fuel cell with the electrolyte layer reinforced with a glass microfiber felt showed excellent electrochemical performance. They found that the solid PWA contained in both experimental layers dissolves during the cell operation. The acid is lost from the cell, the ionic resistance increases and, thus, the electrochemical activity irreversibly decreases. The mechanism of the chemical crossover in a PWA-based fuel cell based was investigated by Giordano et al. [139]. They observed that the electrochemical losses were more significant when the cell was operated at low current density or under open circuit conditions, whereas, the electrochemical activity of the PWA fuel cell appeared to be little affected by the chemical cross-over at high current densities. Staiti et al. [140] found that morphological modifications occur on platinum catalysts during operation in a PWA fuel cell. An increase of platinum particle size with fuel cell operation time was observed on both anodes and cathodes. This phenomenon was significantly larger on the cathode. The uptake of electrolyte by the catalyst layers increased during cell operation. Concurrently, an increase of cell performance was recorded. On the basis of physicochemical characterizations, the growth mechanism of platinum particles was attributed to a dissolution–redeposition phenomenon involving smaller crystallites. The increase of cell performance during the first period of operation was likely due to an increase of the three-phase reaction zone at the electrode–electrolyte interface, whose positive contribution to the cell polarization prevails over the effects of platinum crystallite growth. To overcome the problem of electrolyte dissolution and the consequent short lifetime of the fuel cell, Staiti et al. [141] investigated the possibility of blocking the heteropolyacid in a host material in such a way that it would maintain the high proton conductivity of the original electrolyte. Phosphotungstic and silicotungstic acids were chosen as conductive materials, and silica-gel as supporting material. Silica-supported PWA and SiWA prepared by sol-gel procedure demonstrated that up to 30 wt% of PWA and up to 45 wt% of SiWA can be entrapped within the silica structure and that their thermal stability is substantially enhanced. XRD, IR and DTA analyses of supported HPAs revealed that the usual clathrate structure formed by α-Keggin units interconnected through hydrogen-bonded water molecules in pure acids is replaced by interaction of individual α-Keggin units with silica surface within pores. This interaction was stronger in the case of SiWA than in the case of PWA. Proton conductivities of samples containing 15 and 30 wt% of SiWA were higher with respect to the corresponding samples containing PWA, because the former acid has more protons in the molecule than the latter one.

5.1.2. Tungsten-based HPAs in inorganic–organic membranes for use at temperatures >100 °C

The electrolyte membrane is a basic element in PEMFCs, however, the polymer electrolyte membrane, commonly Nafion®, suffers from degradation at higher temperature, resulting in narrow operational temperature windows below 100 °C. Using an alternative polymer membrane with high stability and sufficient protonic conductivity at temperatures above 100 °C, a PEMFC operating at intermediate temperatures could be realized, overcoming some problems present in the current system, such as CO poisoning. Additionally, DMFCs could operate at intermediate temperatures. Indeed, one of the main drawbacks of DMFCs relies on the slow methanol oxidation kinetics. For this reason, an increase in DMFC operation temperature from 90 to about 150 °C is highly desirable. Organic/inorganic composite membranes with different HPA additives maintain sufficient proton conductivities for atmospheric pressure elevated temperature (>100 °C) PEMFC operation. However, membrane and membrane electrode assembly (MEA) processing is severely curtailed because of the solubility of the HPA additives in water. Indeed, besides HPAs are known to be the most conductive solids among the inorganic solid electrolytes, and they are considered as a new kind of electrolyte for fuel cell applications, however their use as electrolyte material is limited due to their inherent solubility in water [142]. Electrochemically produced water may dissolve HPAs and the acids may leak out through the gas outlet holes, which would result in declining cell performance. Consequently, a major research objective is to fix the HPAs in stable structures and maintain its high proton conductivity. When HPAs were embedded in hydrophilic polymer matrix, they were expected to endow the composite membranes with their high proton conductivity, while retaining the desirable mechanical properties of the polymer membranes.

5.1.2.1. Inorganic–organic membranes with silica stabilized HPAs. Sulfonated polymers are suitable candidates as host materials for PWA since specific interactions between the PWA and the sulfonated polymer are expected. Indeed, Fourier transform infrared (FTIR) spectroscopy band shifts showed that sulfonic acid groups on the polymer backbone interact with both bridging tungstic oxide and terminal tungstic oxide in the PWA molecule, indicative of an intermolecular hydrogen bonding interaction between the copolymer and the additive [143]. The bulk mixing of PWA with Nafion®, sulfonated polysulfone, sulfonated poly(ether ketone ketone), sulfonated poly(ether ether ketone), sulfonated poly(arylene ether sulfone) and sulfonated poly(arylene ether nitrile ketone) leads to hybrid polymer electrolyte membranes with higher ionic conductivity than the pure polymers [144]. However, upon strong membrane hydration and swelling, the dissolution of the PWA in water occurs with detrimental consequences on fuel cells efficiency. Therefore, further stabilization of the PWA is necessary. This can be achieved by anchoring PWA on an oxide support. Silica is a suitable immobilizing agent. Tatsumisago et al. [145] showed that, when PWA is incorporated in a silica-gel film obtained from the sol-gel process of tetraethoxysilane (TEOS), the conductivity at room temperature of the silica gel increased from 10^{-5} to 10^{-3} to 10^{-2} S cm^{-1}. The silica gel has a large number of micropores and mesopores that are "filled" with the proton conductive electrolyte [146]. Strong electrostatic interactions between charged silanol groups

and the polyanions of PWA confer stability to the system [146]. Moreover, the presence of silica provides additional beneficial effects like water retention at high temperatures and reduction of the methanol crossover in DMFCs [144]. When preparing the membrane from solution, the incorporation of silica-supported PWA within a polymeric membrane can be achieved in two ways: via the pre-formation of PWA-silica particles followed by straightforward mixing in a polymer solution [147] or via the *in situ* generation of the inorganic phase within the matrix during film formation, e.g., via the sol gel process of an alkoxide precursor in the presence of PWA [148]. Both methods lead to composite membranes with increased proton conductivity compared to the pure ionomer, especially at low relative humidity (RH).

Nafion®-silica composite membranes doped with PWA and SiWA were investigated for application in intermediate-temperature DMFCs. Staiti et al. [147] tested heteropolyacid-modified Nafion®-silica composite membranes in a DMFC in the temperature range 90–145 °C, and the results were compared with that obtained by a fuel cell using a bare silica-Nafion® recast membrane. The PWA-based membrane showed better electrochemical characteristics at high current densities with respect to both SiWA-modified and silica-Nafion® membranes. Maximum power densities of 400 mW cm^{-2} and 250 mW cm^{-2} were obtained at 145 °C with oxygen and air feed, respectively. The results indicated that the addition of inorganic hygroscopic materials to recast Nafion® extends the DMFC operating range. Similar cell resistance values were observed for these MEAs: this indicates that the enhancement produced by PWA is not related to an increase of electrolyte ionic conductivity, but more likely, it relies on its promoting behavior. In the same way, Shao et al. [149] prepared Nafion®/SiO_2/PWA and Nafion®/SiO_2 composite membranes through the recasting procedure, using Nafion® solution mixed with SiO_2 or PWA/SiO_2. Nafion®/SiO_2/PWA and Nafion®/SiO_2 composite membranes were tested in PEMFCs operated above 100 °C. The incorporation of the inorganic additives PWA and SiO_2 into the Nafion® membrane resulted in enhanced thermal stability and water uptake, besides retaining its inherent property. This hybrid Nafion®-silica membrane doped with PWA exhibited a proton conductivity similar to that of the native Nafion membrane at high temperatures and 100% RH, but much higher at low RH. The single PEMFC with Nafion®/SiO_2/PWA and Nafion®/SiO_2 composite membranes delivered higher current density values (540 and 340 mA cm^{-2} at 0.4 V, respectively) than that of the Nafion® membrane (95 mA cm^{-2}) in the operating conditions of 110 °C and 70% RH. Hydrogen crossover through the composite membranes was much smaller when compared with the Nafion membrane. In a similar work, Ramani et al. [150] investigated Nafion®/SiO_2/PWA composite membranes: the membranes were robust, and demonstrated low H_2 crossover currents of 0.7 mA cm^{-2} for a 25 μm thick membrane. The decomposition onset temperature of the composite membrane was extended by 30 °C over Nafion®. The MEAs, upon subsequent testing in fuel cell environments at 120 °C and 35% RH, indicated that the composite membranes had a slightly (15%) superior conductivity when compared to recast Nafion®.Sulfonated poly(ether ether ketone) (SPEEK) is a highly hydrophilic polymer with fairly good conductivity. With the good thermal stability and mechanical strength as well as adequate conductivity, SPEEK is a good candidate for DMFC applications. However, the conductivity of SPEEK membrane is still lower than that of Nafion®. Its proton conductivity depends on the degree of sulfonation (DS). However, the mechanical properties tend to deteriorate as the DS increases. Highly sulfonated polymers will swell significantly at high temperature and humidity. Thus, to increase the proton conductivity without deteriorate the mechanical strength, the trend is to use SPEEK with low DS doped with silica-incorporated HPAs. Fu et al. [151] prepared SPEEK/aminopropyltriethoxysilane (KH550) hybrid membranes doped with different PWA amount by a casting procedure. Interaction between amine groups in KH550 and sulfonic acid groups in SPEEK occurred and the crosslinked silica network not only improved the stability, water retention and mechanical strength of membranes but also immobilized the PWA molecules in the polymer matrix with non-covalent bond. The proton conductivity of the hybrid membrane with 5 wt% PWA for SPEEK/KH550 reached the maximum of 8.4×10^{-2} S cm^{-1} at 25 °C and 16×10^{-2} S cm^{-1} at 80 °C under 100% RH condition. Colicchio et al. [144] prepared SPEEK/SiO_2/PWA composite membranes. The silica was generated *in situ* via the water free sol-gel process of polyethoxysiloxane (PEOS), a liquid hyperbranched inorganic polymer of low viscosity. At 100 °C and 90% RH the membrane prepared with PEOS (silica content = 20 wt%) showed two times higher conductivity than the pure SPEEK. The addition of small amounts of PWA (2 wt% of the total solid content), introduced in the early stage of membrane preparation, resulted in a further increase in conductivity (more than three times the pure SPEEK). During membrane formation, PWA and $-SO_3H$ groups of SPEEK acted as catalysts in the conversion of PEOS in silica. Ismail et al. [152] prepared composite membranes formed by a SPEEK and SiWA loaded on a silica-aluminium oxide (SiO_2-Al_2O_3) composite. SiWA was fixed on the composite oxide, so that it became insoluble in water. The membranes possessing higher sulfonation degree, higher SiWA content and higher SiO_2 content in SiO_2-Al_2O_3 composite showed higher water uptake and proton conductivity. The water uptake of SPEEK/SiO_2-Al_2O_3/PWA membranes was higher than that of the Nafion® 112 membrane. The methanol permeability of composite membrane decreased with increasing the sulfonation degree. With increasing SiO_2 content in SiO_2-Al_2O_3, the methanol permeability also increased, but the value was still lower than Nafion® 112.

Instead of sulfonate polymers, the group of Honma used polyethers polymers to synthesize hybrid membrane [148,153–159]. Inorganic parts such as silicate or metal (Zr,Ti) alkoxides are reactive, so they can be directly cross-linked to organic parts such as polydimethylsiloxane (PDMS) and polyether polymers (polyethylene oxides, polypropylene oxide, polytetramethylene oxide (PTMO), etc.) by hydrolysis and condensation reactions. The organic–inorganic interfaces can be formed by sol-gel processing of end groups of organic parts with reactive inorganic parts to afford hybrids at molecular scale. Moreover the hybrid material becomes proton-conducting electrolytes by incorporation of HPAs, where nanostructured macromolecules provide fast proton-conducting pathways by assembling PWA clusters or chemical bonding at inorganic hydrophilic interfaces. Commonly PWA is a good candidate material for being incorporated by sol-gel processes. Polyanion PWA clusters were incorporated with inorganic silica framework and they never dissociated from the hybrid matrix. These hybrid organic–inorganic proton conductor materials showed thermal stability up to 300 °C due to the presence of cross-linkable inorganic nanophase in the hybrid macromolecular matrix, and the maximum proton conductivity of 8×10^{-2} S cm^{-1} under saturated humidity condition at 150 °C for TiO_2/PTMO/PWA [148].

5.1.2.2. Other methods to PWA stabilization in composite membranes. Ramani and co-workers investigated Nafion®-based organic/inorganic composite membranes with different HPA additives as alternate materials for low humidity PEFC operation [160–163]. They observed that two major factors limiting the performance of Nafion®/HPA composite membranes are (1) the extremely high solubility of the HPA additive in aqueous media and (2) the large particle size of the inorganic additive within the Nafion® matrix, which in turn results in ineffective bridging

between the ionic domains [160,161]. Indeed, they proposed that the role of HPA additives in the composite membrane is to reduce R_h (resistance to transport via hopping)), at high temperatures and low RHs, resulting in reduced membrane resistance. For the effectiveness of the additive, the particle size should be on the order of a few nanometers, to effectively bridge the shrunken clusters in Nafion®. If the particle sizes are large, the dispersion of the additive will be poor and only a minimal number of clusters will be bridged. Such a scenario should result in next to no improvement in proton conductivities at low humidity [160]. To reduce PWA dissolution, Ramani et al. [161] fabricated composite membranes with the PWA additive rendered insoluble by ion exchanging protons with larger cations such as Cs^+, NH_4^+, Rb^+ and Tl^+. The additive loss in aqueous media was lowered from nearly 100% (unmodified PWA) to about 5% (modified PWA). The membranes were robust, and demonstrated low H_2 crossover currents of around 2 mA cm^{-2} for a 28 μm thick membrane. All membranes were evaluated at high temperatures and low RHs in an operating fuel cell. The MEAs demonstrated stable performance for several hours. The conductivities of the composite membranes at 120 °C and 35% RH were around 1.6×10^{-2} S cm^{-1}. In a nest work, Ramani et al. [162] reduced the PWA particle size by nearly two orders of magnitude from 1 to 2 μm to 30 nm by modifying the casting procedure. The composite membranes had crossover currents on the order of 1–5 mA cm^{-2}, with the crossover flux decreasing and approaching the value for recast Nafion® as the particle size was reduced. A 25 μm thick composite membrane with large additive particles had an area-specific resistance of 0.22 Ω cm^{-2} at 120 °C and 35% RH, while the corresponding value for a 25 μm thick membrane with small additive particles was 0.16 Ω cm^{-2}. The latter membrane compared favorably with recast Nafion®, which has an area-specific resistance of 0.19 Ω cm^{-2}. Next, they combined the previously described existing PWA additive and MEA stabilization techniques to yield a stabilized MEA for operation at 120 °C and 35% RH [163]. MEAs were prepared using Nafion®/PWA composite membranes with a PWA particle size of 30–50 nm. The PWA additive was stabilized by substituting its protons with cesium counter ions. The Nafion® in the membrane and electrodes was simultaneously converted to the Cs^+ form by an ion-exchange process. The melt processability of the Nafion® in the Cs^+ form permitted the MEA to be heat treated at 200 °C and 30atm, promoting the development of a durable membrane/electrode interface. The prior stabilization of the PWA permitted MEA re-protonation with minimal additive loss. The stabilization process did not affect the integrity of the MEA, with the hydrogen crossover currents through the membrane remaining unchanged at 2 mA cm^{-2}.

Generally, oppositely charged polyions (polycations or polyanions) interact electrostatically to form polyelectrolyte complexes. Chitosan is a natural and low-cost biopolymer with unique properties such as biocompatibility, nontoxicity, chemical and thermal stability, and has been widely studied as a promising source of membrane materials. As a kind of polycation, chitosan is extremely attractive to prepare polyelectrolyte complexes through electrostatic interactions with polyanions. The acids and salts of heteropolyanions constitute a large category of compounds, thus a variety of polyelectrolyte complexes would be formed between heteropolyanions and chitosan. Thus, another way to resolve the problem of HPA dissolution during fuel cell operation could be the introduction of electrostatic interactions between chitosan and HPAs. It has been found that the mixing of chitosan solution and HPA solution leads to the formation of insoluble complexes. Therefore, HPAs could be immobilized in the membranes through electrostatic interaction. On these bases, Cui et al. [164] prepared polyelectrolyte complexes (PECs) of chitosan and PWA and evaluated the possibility of their use as novel proton-conducting membranes for DMFCs. The homogeneous PECs membranes showed good thermal stability up to 210 °C, and exhibited a high proton conductivity (2.4×10^{-2} S cm^{-1} at 80 °C) and a low methanol permeability (3.3×10^{-7} cm^2 s^{-1}).

5.1.3. Anhydrous PWA-containing proton-conducting membranes

The proton transport under anhydrous conditions might be based on a non-vehicular mechanism (Grotthuss mechanism), in which only protons are mobile from site to site without the assistance of diffusible vehicle molecules, such as water molecules. The activation energy of this type of proton transport can primarily depend on the distance between the hopping sites. Therefore, acid–base composite materials have been the primary focus for the anhydrous proton conductive materials. The acidic and basic molecules act as proton donors and acceptors during the proton-transfer reactions, respectively. Namely, the proton transfer is controlled by the ΔpK_a value. Therefore, a similar transfer reaction might occur at not only the acid–base composite but also the acid–acid composite materials, which are composed of acidic and strong-acidic molecules, such as heteropolyacids. On these bases, Yamada and Honma [165] investigated the proton-conducting structure and mechanism of a PWA-sulfonic acid (PSS) composite material. Surprisingly, this material formed a PWA-encapsulated structure by the self-assembly of $-SO_3H$ onto the PWA surface and had the high anhydrous proton conductivity of 1×10^{-2} S cm^{-1} at 180 °C. Additionally, test using a nonhumidified H_2/O_2 fuel cell demonstrated power generation at 160 °C. These anhydrous proton-conducting materials operating without the presence of water molecules are quite different from the commonly used ion-exchange membrane, and may have advantages as an electrolyte membrane for PEMFCs operating at intermediate temperatures under anhydrous conditions. They proposed a novel anhydrous proton-conducting structure and mechanism for the PSS–PWA composite. Since the acidity of the molecule is based on the p*K*a value, the PWA and PSS molecules are a Brønsted acid and base, respectively. Therefore, the proton of PWA jumps to $-SO_3H$ in PSS and the proton defect site was constructed on the PWA surface; as a result, the free proton from the PWA molecule interacts with the $-SO_3H$ and forms $-SO_3H_2^+$. Additionally, the proton in $-SO_3H_2^+$ was slightly attracted to the PWA surface to compensate for the proton defect of PWA. Furthermore, since the $-SO_3H$ group has been fixed in the backbone of PSS chain, it constructs the closest packing structure on PWA surface.

Besides inorganic conductors, ionic liquids, which have high ionic conductivities over a wide temperature range, non-volatility, thermal stability and non-flammability, have been investigated for use in batteries and fuel cells. Noda et al. [166] reported Bronsted acid–base ionic liquids as proton conducting nonaqueous electrolytes. Among them, bis-(trifluoromethanesulfonyl) amide (TFSI)/imidazole in a molar ratio of 1 showed high thermal stability up to 300 °C. These ionic liquids possibly form a channel, which acts as a fast proton conducting path, by replacing water under anhydrous conditions. Thus, Kim et al. [167,168] synthesized a molecular hybrid conductor electrolyte using PWA and [1-butyl-3-methylimidazole][bis-(fluoromethanesulfonyl) amide] ([BMIM][TFSI]) ionic liquid, and investigated the conductivity of PWA-[BMIM][TFSI] hybrids under anhydrous conditions. In these new hybrids, there was a strong interaction between $[BMIM]^+$ of the ionic liquid and PWA. The hybrids were very stable up to about 400 °C and showed a high ion jump during heating and cooling processes. It was concluded that the ion jump was due to melting and solidification of the hybrid. The hybrid crystallized in the orthorhombic space group $Pca2_1$, and the chemical formula of the hybrid in the single crystal was $PW_{13}C_{32}H_{56}O_{54}N_8S_{0.16}F_{0.26}$. The PWA-[BMIM][TFSI] hybrids kept water molecules, exceeding six H_2O molecules, in the hybrid molecular structure. The hybrids sup-

pressed the loss of water from the PWA-[BMIM][TFSI] molecular structure up to 80 °C and showed a high conductivity (4×10^{-2} S cm^{-1} at 60 °C). The high conductivity can be due to the protonic carriers. However, long term durability test showed that ionic liquid could undergo some degradation under anhydrous conditions.

5.2. $WO_3 \cdot 2H_2O$

It is well known that some metal oxide hydrates like $Sb_2O_5 \cdot nH_2O$, $ZrO_2 \cdot nH_2O$ and $SnO_2 \cdot nH_2O$ show considerably high proton conductivity [169]. It is possible to classify these compounds into two categories, the lattice hydrates and the particle hydrates. In the lattice hydrates the water molecules are strongly bound to the lattice and the water composition as well as the conductivity remains stable until low RHs. In the case of particle hydrates where the conductivity is related to adsorbed species, the conductivity strongly depends on the partial pressure of water [170]. Proton conductivity of $WO_3 \cdot 2H_2O$, a lamellar hydrate, was investigated in a wide range of temperature from 0 to 150 °C by Li et al. [171]. Its conductivity at 150 °C was in the order of 10^{-2} S cm^{-1} and retained at this high level until the compound was decomposed into monohydrate at the water pressure around $p_{H2O}/p_s = 0.65$. It seems that, in the higher temperature region, the proton is transported by a bulk mechanism with the help of a hydrogen bond network system formed by coordinated and inter-layer water molecules between $WO_3[H_2O]$ layers. From a practical point of view, $WO_3 \cdot 2H_2O$ would be potentially useful as a proton conducting solid electrolyte for fuel cells operated at intermediate temperatures.

For practical use in fuel cells, the electrolyte material must be in the form of flexible film. In this respect, inorganic/organic composites are suitable. In the composite films, inorganic particles must be dispersed homogeneously to form conduction paths. However, as these kinds of oxides have little solubility in water or organic solvents, homogeneous mixture into organic polymer is difficult, and the preparation of homogeneous membrane also becomes difficult. Such dispersion is difficult to attain by simple mixing of inorganic powders with polymers. To obtain well-dispersed composites, Tanaka et al. [172] developed the "precursor mixing method": precursors of both inorganic and organic components are mixed in the liquid phase and the inorganic component is precipitated within the hardened organic component. They prepared $WO_3 \cdot 2H_2O$/epoxy resin composite films by the precursor mixing method, and the proton conduction properties of the composite films were evaluated at 20–80 °C under saturated water vapor pressure. The composite films with 16–40 vol% $WO_3 \cdot 2H_2O$ had large primary and secondary particles of $WO_3 \cdot 2H_2O$ compared with $WO_3 \cdot 2H_2O$ powders obtained by hydrolysis of Na_2WO_4 solution. The proton conductivity at 50 °C under saturated water vapor pressure increased abruptly with $WO_3 \cdot 2H_2O$ content, reaching the value of $WO_3 \cdot 2H_2O$ powder compact at 16 vol%. The conductivity of the film with 40 vol% $WO_3 \cdot 2H_2O$ was 6.3×10^{-4} S cm^{-1}, which is higher than that of $WO_3 \cdot 2H_2O$ powder compact. The bulk conduction mechanism through the hydrogen bond network of $WO_3 \cdot 2H_2O$ was suggested to be dominant above 40 °C. The large primary particles and fully connected secondary particles of $WO_3 \cdot 2H_2O$ were assumed to contribute effectively to proton migration in the composite films.

Yang et al. [173] prepared WO_3/perfluorosulfonic acid (PFSA) membranes, in the weight ratio WO_3/PFSA = 8 and 15 wt%, by recasting the PFSA ionomer dispersion and the WO_3 precursor solution. The results proved that the resistances of the WO_3-containing membranes in fuel cells are significantly lower than that of the fuel cell with Nafion® 112 membrane. The performances of PEMFCs with WO_3/PFSA membranes were superior to that of the cell with Nafion® 112. The cell with the 15 wt% WO_3/PFSA membrane better performed than that with the 8 wt% WO_3/PFSA membrane.

The characteristics of composite membranes with tungsten-based proton conducting materials are summarized in Table 2.

Table 2
Physical, physico-chemical and electrochemical properties of tungsten-containing composite membranes.

Tungsten-containing composite membrane	Physical, physico-chemical and electrochemical properties	References
Nafion®/SiO_2/PWA(SiWa)	High stability above 100 °C Low H_2 crossover Proton conductivity similar to that of Nafion® membrane at high temperatures and 100% RH, but much higher at low RH High performance in PEMFCs and DMFCs	[147–150]
SPEEK/KH550/PWA, SPEEK/SiO_2/PWA, SPEEK/SiO_2-Al_2O_3/PWA	Maximum of proton conductivity of 8.4×10^{-2} S cm^{-1} at 25 °C and 16×10^{-2} S cm^{-1} at 80 °C under 100% RH condition for SPEEK/KH550/PWA Higher stability, water uptake and proton conductivity, and lower methanol permeability of SPEEK/SiO_2-Al_2O_3/PWA than Nafion® 112	[144,151,152]
Polyether-based hybrid membranes	Thermal stability up to 300 °C Maximum proton conductivity of 8×10^{-2} S cm^{-1} under saturated humidity condition at 150 °C for PTMO/TiO_2/PWA	[148,153–159]
Nafion®/Cs^+(NH_4^+,Rb^+,Tl^+)-modified PWA	Low PWA dissolution Low H_2 crossover Proton conductivity at 120 °C and 35% RH 1.6×10^{-2} S cm^{-1} Stable PEMFC performance for several hours	[161]
Nafion®/small-particle-size-PWA	Area-specific resistance at 120 °C and 35% RH of a 25 μm thick Nafion®/PWA with small PWA particles 0.16 Ω cm^{-2}, while with large PWA particles 0.22 Ω cm^{-2} Area-specific resistance of recast Nafion® 0.19 Ω cm^{-2}	[162]
Polyelectrolyte complexes (PECs) of chitosan and PWA	Thermal stability up to 210 °C High proton conductivity (2.4×10^{-2} S cm^{-1} at 80 °C) Low methanol permeability (3.3×10^{-7} cm^2 s^{-1})	[164]
Anhydrous PSS–PWA membrane	Proton conductivity 1×10^{-2} S cm^{-1} at 180 °C Power generation of a non-humidified H_2/O_2 fuel cell at 160 °C	[165]
Anhydrous PWA-[BMIM][TFSI] hybrids	Stable up to about 400 °C No loss of water up to 80 °C High proton conductivity (4×10^{-2} S cm^{-1} at 60 °C)	[167,168]
WO_3/PFSA (8 and 15 wt% WO_3)	Lower resistances of the WO_3/PFSA membranes in fuel cells than that of the fuel cell with Nafion® 112 membrane. Performances of PEMFCs with WO_3/PFSA membranes superior to that of the cell with Nafion® 112	[173]

Table 3
Tungsten-based materials and their main use in fuel cells.

W-based materials	Use/reaction	Fuel cell type	References.
M_xWO_3	Cathode catalyst/ORR	Acid FC	[12–15]
W_xC	Anode catalyst/HOR,MOR	PEMFC,DMFC,MFC	[17–46]
	Co-catalyst/HOR,MOR,EOR,ORR	PEMFC,DMFC,DEFC	[77–93]
	Catalyst support/MOR,ORR	PEMFC,DMFC	[124–134]
W_2N	Cathode catalyst/ORR	PEMFC	[47]
WO_x	Co-catalyst/HOR,MOR,EOR	PEMFC,DMFC,DEFC	[49–76]
	Catalyst support/MOR	DMFC	[119–122]
	Electrolyte	PEMFC	[171–173]
PtW, PtRuW alloys	Co-catalyst/ORR,MOR,EOR	PEMFC,DMFC,DEFC	[95–100]
WO_4^{2-}	Co-catalyst/ORR	MCFC	[114–117]
PWA, SiWA	Co-catalyst/HOR/CO,ORR,MOR	PEMFC,DMFC	[67,105–112]
	Electrolyte	PEMFC,DMFC	[137–168]

6. Conclusions

Tungsten-based materials can be used as catalysts, co-catalysts, catalyst support and electrolytes in various types of fuel cells. Tungsten-based anode and cathode catalysts and co-catalysts, catalyst supports and composite membrane can be used in polymer membrane fuel cells fuelled with either hydrogen or low molecular weight alcohols. Tungsten carbide fulfills the requirements for the use as anode catalyst in microbial fuel cells. The addition of potassium tungstate to nickel anode increases the performance of molten carbonate fuel cells as well as the addition of K_2WO_4 to the electrolyte of an MCFC improves the stability of lithium aluminate, the state-of-the-art matrix support material. The different tungsten-based compounds and their use in fuel cells are reported in Table 3.

The most promising tungsten-based materials and their use in fuel cells are the following:

1. WO_3 as co-catalyst in ternary Pt-Ru-WO_3 anode catalysts with higher MOR activity than Pt-Ru.
2. W_2C as co-catalysts in Pt-W_2C/C cathode catalysts with higher ORR than Pt/C.
3. WO_3 and W_xC as stable carbon-alternative catalyst supports.
4. PWA as proton conducting electrolyte in membranes for use in intermediate temperature fuel cells.

On these bases, a DMFC operating at temperature >100 °C can be assembled by using tungsten-containing materials as catalysts and electrolyte membrane:

Anode: WO_3 and W_xC supported Pt. The tungsten-based supports are more stable at high temperature than carbon supports. Moreover, they present higher MOR activity than PtRu/C [119,121,130,132].

Cathode: Three types of tungsten-containing catalysts can be used as cathode material. (1) Pt supported on WC microspheres [131]: high stability at high temperature of the support and higher ORR activity than Pt/C. (2) Carbon supported methanol tolerant Pt-W_2C [91,93] or highly stable PtW alloy [95,96]: higher ORR activity than Pt/C. Both these catalysts allow the decrease of Pt content in the cell without sacrificing the fuel cell performance. (3) Carbon supported PdW alloy [103]: this catalyst has the same ORR activity than that of Pt, but with higher methanol tolerance.

To increase the ORR activity, the use of PWA-modified Nafion®-stabilized inks of the catalyst to prepare the catalytic layer of the electrode is suggested.

Membrane: SPEEK/SiO_2-Al_2O_3/PWA [152], titania/PTMO/PWA [148] and chitosane/PWA [164]: these composite membranes are stable and with high proton conductivity at temperature >100 °C and have lower methanol permeability than Nafion®.

Acknowledgment

The authors thank the Conselho Nacional de Desenvolvimento Científico e Tecnológico (CNPq, Proc. 310151/2008-2) for financial assistance to the project.

References

[1] J.E. Emsley, The Elements, 2nd ed., Oxford University Press, New York, 1991.
[2] B.S. Hobbs, A.C.C. Tseung, J. Electrochem. Soc. 122 (1975) 1174–1177.
[3] M.A. Butler, J. Appl. Phys. 48 (1977) 1914–1920.
[4] CRC Handbook of Chemistry and Physics, 67th ed. (1986-1987), CRC Press, Inc., Boca Raton, FL, 1987, p. B-141.
[5] M. Pourbaix, Atlas of Electrochemical Equilibria in Aqueous Solutions, Pergamon, London, 1966, p. 280.
[6] R.V. Sara, J. Am. Ceram. Soc. 48 (1965) 251–257.
[7] L. Bennett, J.R. Cuthill, A. McAlister, N. Erickson, R. Watson, Science 187 (1975) 858–859.
[8] G.A. Tsirlina, O.A. Petrii, Electrochim. Acta 32 (1987) 637–647.
[9] K.M. Andersson, L. Bergström, Int. J. Refractory Metals Hard Mater. 18 (2000) 121–129.
[10] B. Bozzini, G.P. De Gaudenzi, A. Fanigliulo, C. Mele, Corrosion Sci. 46 (2004) 453–469.
[11] P. Hagenmuller, Progr. Solid State Chem. 5 (1971) 71–114.
[12] D.B. Sepa, A. Damianovic, J.O'M. Bockris, Electrochim. Acta 12 (1967) 746–747.
[13] J.O'M. Bockris, J. McHardy, J. Electrochem. Soc. 120 (1973) 61–66.
[14] J. McHardy, J.O'M. Bockris, J. Electrochem. Soc. 120 (1973) 53–60.
[15] B. Broyde, J. Catal. 10 (1968) 13–18.
[16] R.D. Armstrong, A.F. Douglas, D.E. Williams, Energy Convers. 11 (1971) 7–10.
[17] H. Binder, A. Kohling, W. Kuhn, W. Lindner, G. Sandstede, Nature 224 (1969) 1299–1300.
[18] D. Baresel, W. Gellert, J. Heidemeyer, P. Scharner, Angew. Chem. Int. Ed. 10 (1971) 194–195.
[19] R.B. Levy, M. Boudart, Science 181 (1973) 547–549.
[20] V.Sh. Palanker, D.V. Sokolsky, E.A. Mazulevsky, E.N. Baybatyrov, J. Power Sources 1 (1976/77) 169–176.
[21] P.N. Ross, P. Stonehart, J. Catal. 48 (1977) 42–59.
[22] I. Nikolov, V. Nikolova, T. Vitanov, M. Svatá, J. Power Sources 4 (1979) 65–75.
[23] I. Nikolov, T. Vitanov, J. Power Sources 5 (1980) 273–281.
[24] I. Nikolov, T. Vitanov, J. Power Sources 5 (1980) 283–290.
[25] V.Sh. Palanker, R.A. Gajyev, D.V. Sokolsky, Electrochim. Acta 22 (1977) 133–136.
[26] D.R. McIntyre, G.T. Burstein, A. Vossen, J. Power Sources 107 (2002) 67–73.
[27] X.G. Yang, C.Y. Wang, Appl. Phys. Lett. 86 (2005) 224104–224112.
[28] C.D.A. Brady, E.J. Rees, G.T. Burstein, J. Power Sources 179 (2008) 17–26.
[29] E.J. Rees, K. Essaki, C.D.A. Brady, G.T. Burstein, J. Power Sources 188 (2009) 75–81.
[30] M. Nagai, M. Yoshida, H. Tominaga, Electrochim. Acta 52 (2007) 5430–5436.
[31] S. Izhar, M. Yoshida, M. Nagai, Electrochim. Acta 54 (2009) 1255–1262.
[32] K. Lee, A. Ishihara, S. Mitsushima, N. Kamiya, K. Ota, Electrocim. Acta 49 (2004) 3479–3485.
[33] H. Okamoto, G. Kawamura, A. Ishikawa, T. Kudo, J. Electrochem. Soc. 134 (1987) 1645–1649.
[34] G. Kawamura, H. Okamoto, A. Ishikawa, T. Kudo, J. Electrochem. Soc. 134 (1987) 1653–1658.
[35] H.H. Hwu, J.G. Chen, K. Kourtakis, G. Lavin, J. Phys. Chem. B 105 (2001) 10037–10044.
[36] H.H. Hwu, B.D. Polizzotti, J.G. Chen, J. Phys. Chem. B 105 (2001), 10037 10045-10053.
[37] H.H. Hwu, J.G. Chen, J. Phys. Chem. B 107 (2003) 2029–2039.
[38] H.H. Hwu, J.G. Chen, J. Vacuum Sci. Tech. A 21 (2003) 1488–1493.
[39] E.C. Weigert, M.B. Zellner, A.L. Stottlemyer, J.G. Chen, Topics Catal. 46 (2007) 349–357.
[40] H. Lu, T. Yan, J. Wuhan University Tech. Mater. 24 (2009) 229–234.

[41] E. Miyazaki, I. Kojima, M. Orita, J. Chem. Soc. Chem. Comm. (1985) 108–109.
[42] C.A. Angelucci, L.J. Deiner, F.C. Nart, J. Solid state Electrochem. 12 (2008) 1599–1603.
[43] C.J. Barnett, G.T. Burstein, A.R.J. Kucernak, K.R. Williams, Electrochim. Acta 42 (1997) 2381–2388.
[44] M. Rosenbaum, F. Zhao, U. Schröder, F. Scholz, Angew. Chem. Int. Ed. 45 (2006) 6658–6661.
[45] M. Rosenbaum, F. Zhao, M. Quaas, H. Wulff, U. Schröder, F. Scholz, Appl. Catal. B 74 (2007) 261–269.
[46] F. Harnisch, U. Schröder, M. Quaas, F. Scholz, Appl. Catal. B 87 (2009) 63–69.
[47] H. Zhong, H. Zhang, Y. Liang, J. Zhang, M. Wang, X. Wang, J. Power Sources 164 (2007) 572–577.
[48] P.K. Shen, K.Y. Chen, A.C.C. Tseung, J. Chem. Soc., Faraday Trans. 90 (1994) 3089–3096.
[49] A.C.C. Tseung, P.K. Shen, K.Y. Chen, J. Power Sources 61 (1996) 223–225.
[50] K.W. Park, K.S. Ahn, J.H. Choi, Y.C. Nah, Y.M. Kim, Y.E. Sung, Appl. Phys. Lett. 81 (2002) 907–909.
[51] S. Jayaraman, T.F. Jaramillo, S.-H. Baeck, E.W. McFarland, J. Phys. Chem. B 109 (2005) 22958–22966.
[52] V. Raghuveer, B. Viswanathan, J. Power Sources 144 (2005) 1–10.
[53] F. Maillard, E. Peyrelade, Y. Soldo-Olivier, M. Chatenet, E. Chaînet, R. Faure, Electrochim. Acta 52 (2007) 1958–1967.
[54] J. Shim, C.-R. Lee, N.-K. Lee, J.-S. Lee, E.J. Cairns, J. Power Sources 102 (2001) 172–177.
[55] C. He, H.R. Kunz, J.M. Fenton, J. Electrochem. Soc. 150 (2003) A1017.
[56] J.E. Benson, H.W. Kohn, M. Boudart, J. Catal. 5 (1966) 307–313.
[57] B.S. Hobbs, A.C.C. Tseung, Nature 222 (1969) 556–558.
[58] B.S. Hobbs, A.C.C. Tseung, J. Electrochem. Soc. 119 (1972) 580–583.
[59] B.S. Hobbs, A.C.C. Tseung, J. Electrochem. Soc. 120 (1973) 766–769.
[60] B.S. Hobbs, A.C.C. Tseung, J.Electrochem. Soc. 122 (1975) 1174–1177.
[61] L.W. Niedrach, I.B. Weinstock, Electrochem. Technol. 3 (1965) 270–274.
[62] P.J. Kulesza, L.R. Faulkner, J. Electroanal. Chem. 259 (1989) 81–98.
[63] P.K. Shen, A.C.C. Tseung, J. Electrochem. Soc. 141 (1994) 3082–3090.
[64] A.K. Shukla, M.K. Ravikumar, S. Arico, G. Candiano, V. Antonucci, N. Giordano, A. Hamnett, J. Appl. Electrochem. 25 (1995) 528–532.
[65] L. Colmenares, Z. Jusys, S. Kinge, H. Boennemann, R.J. Behm, J. New Mater. Electrochem. Syst. 9 (2006) 107–120.
[66] L.X. Yang, C. Bock, B. MacDougall, J. Park, J. Appl. Electrochem. 34 (2004) 427–438.
[67] L.G.S. Pereira, F.R. dos Santos, M.E. Pereira, V.A. Paganin, E.A. Ticianelli, Electrochim. Acta 51 (2006) 4061–4066.
[68] P.J. Barczuk, H. Tsuchiya, J.M. Macak, P. Schmuki, D. Szymanska, O. Makowski, K. Miecznikowski, P.J. Kulesza, Electrochem. Solid State Lett. 9 (2006) E13–16.
[69] M. Götz, H. Wendt, Electrochim. Acta 43 (1998) 3637–3644.
[70] K. Lasch, L. Jörissen, J. Garche, J. Power Sources 84 (1999) 225–230.
[71] E. Antolini, Appl. Catal. B 74 (2007) 337–350.
[72] K.W. Park, K.S. Ahn, J.H. Choi, Y.C. Nah, Y.M. Kim, Y.E. Sung, Appl. Phys. Lett. 82 (2003) 1090–1092.
[73] M.K. Jeon, K.R. Lee, S.I. Woo, Kor. J. Chem. Eng. 26 (2009) 1028–1033.
[74] W. Zhou, Z. Zhou, S. Song, W. Li, G. Sun, P. Tsiakaras, Q. Xin, Appl. Catal. B 46 (2003) 273–285.
[75] P. Strasser, Q. Fan, M. Devenney, W.H. Weinberg, P. Liu, J.K. Norskov, J. Phys. Chem. B 107 (2003) 11013–11021.
[76] P.K. Shen, J. Syed-Bokhari, A.C.C. Tseung, J. Electrochem. Soc. 138 (1991) 2778–2783.
[77] R. Venkataraman, H.R. Kunz, J.M. Fenton, J. Electrochem. Soc. 150 (2003) A278–A284.
[78] L.G.R.A. Santos, K.S. Freitas, E.A. Ticianelli, J. Solid State Electrochem. 11 (2007) 1541–1548.
[79] M.K. Jeon, K.R. Lee, W.S. Lee, H. Daimon, A. Nakahara, S.I. Woo, J. Power Sources 185 (2008) 927–931.
[80] G.K. Wolf, R. Spiegel, K. Zucholl, Nucl. Instr. Meth. Phys. Res. B 19/20 (1987) 1030–1033.
[81] N. Liu, K. Kourtakis, J.C. Figueroa, J.G. Chen, J. Catal. 215 (2003) 254–263.
[82] M.B. Zellner, J.G. Chen, Catal. Today 99 (2005) 299–307.
[83] Z.J. Mellinger, E.C. Weigert, A.L. Stottlemyer, J.G. Chen, Electrochem. Solid State Lett. 11 (2008) B63–B67.
[84] Z. Zhao, X. Fang, Y. Li, Y. Wang, P.K. Shen, F. Xie, X. Zhang, Electrochem. Comm. 11 (2009) 290–293.
[85] G. Lu, J.S. Cooper, P.J. McGinn, J. Power Sources 161 (2006) 106–114.
[86] F.P. Hu, P.K. Shen, J. Power Sources 173 (2007) 877–881.
[87] J. Kim, J.-H. Jang, Y.-H. Lee, Y.-U. Kwon, J. Power Sources 193 (2009) 441–446.
[88] H. Meng, P.K. Shen, Chem. Comm. (2005) 4408-4410, doi:10.1039/b506900a.
[89] H. Meng, P.K. Shen, Electrochem. Comm. 8 (2006) 588–594.
[90] M. Nie, P.K. Shen, Z. Wei, J. Power Sources 167 (2007) 69–73.
[91] H. Meng, P.K. Shen, J. Phys. Chem. B 109 (2005) 22705–22709.
[92] M. Nie, P.K. Shen, M. Wu, Z. Wei, H. Meng, J. Power Sources 162 (2006) 173–176.
[93] H. Meng, P.K. Shen, Z. Wei, S.P. Jiang, Electrochem. Solid State Lett. 9 (2006) A368–A372.
[94] R. Wang, C. Tian, L. Wang, B. Wang, H. Zhang, H. Fu, Chem. Comm. (2009) 3104–3106.
[95] T. He, E. Kreidler, L. Xiong, J. Luo, C.J. Zhong, J. Electrochem. Soc. 153 (2006) A1637–A1643.
[96] L. Xiong, T. He, Electrochem. Comm. 8 (2006) 1671–1676.
[97] L. Xiong, T. He, USPTO Patent Application 20080008924.
[98] Z.-B. Wang, P.-J. Zuo, G. Ping Yin, J. Alloys Comp. 479 (2009) 395–400.
[99] M. Umeda, H. Ojima, M. Mohamedi, I. Uchida, J. Power Sources 136 (2004) 10–15.
[100] S. Tanaka, M. Umeda, H. Ojima, Y. Usui, O. Kimura, I. Uchida, J. Power Sources 152 (2005) 29–34.
[101] H. Cheng, W. Yuan, K. Scott, D.J. Browning, J.B. Lakeman, Appl. Catal. B 75 (2007) 221–228.
[102] H. Cheng, W. Yuan, K. Scott, D.J. Browning, J.B. Lakeman, J. Power Sources 172 (2007) 597–603.
[103] A. Sarkar, A.V. Murugan, A. Manthiram, J. Mater. Chem. 19 (2009) 159–165.
[104] M.T. Pope, Heteropoly and Isopoly Oxometallates, Springer, NewYork, 1983.
[105] P.J. Kulesza, K. Karnicka, K. Miecznikowski, M. Chojak, A. Kolary, P.J. Barczuk, G. Tsirlina, W. Czerwinski, Electrochim. Acta 50 (2005) 5155–5162.
[106] R. Wlodarczyk, M. Chojak, K. Miecznikowski, A. Kolary, P.J. Kulesza, R. Marassi, J. Power Sources 159 (2006) 802–809.
[107] R. Wlodarczyk, A. Kolary-Zurowska, R. Marassi, M. Chojak, P.J. Kulesza, Electrochim. Acta 52 (2007) 3958–3964.
[108] M. Chojak, A. Kolary-Zurowska, R. Wlodarczyk, K. Miecznikowski, K. Karnicka, B. Palys, R. Marassi, P.J. Kulesza, Electrochim. Acta 52 (2007) 5574–5581.
[109] H. Nakajima, I. Honma, Electrochem. Solid State Lett. 7 (2004) A135–A137.
[110] M. Chojak, M. Mascetti, R. Wlodarczyk, R. Marassi, K. Karnicka, K. Miecznikowski, P.J. Kulesza, J. Solid State Electrochem. 8 (2004) 854–860.
[111] J.R. Farrell III, M.-C. Kuo, J.A. Turner, A.M. Herring, Electrochim. Acta 53 (2008) 4927–4933.
[112] T. Maiyalagan, Int. J. Hydr. En. 34 (2009) 2874–2879.
[113] S. Terada, K. Higaki, I. Nagashima, Y. Ito, J. Power Sources 83 (1999) 227–230.
[114] H. Yabe, Y. Ito, K. Ema, J. Oishi, J. Power Sources 24 (1988) 207–214.
[115] G. Xie, K. Ema, Y. Ito, J. Power Sources 35 (1991) 123–130.
[116] S. Terada, I. Nagashima, K. Higaki, Y. Ito, J. Power Sources 75 (1998) 223–229.
[117] S. Terada, K. Higaki, I. Nagashima, Y. Ito, J. Power Sources 83 (1999) 178–185.
[118] H. Chhina, S. Campbell, O. Kesler, J. Electrochem. Soc. 154 (2007) B533–B539.
[119] R. Ganesan, J.S. Lee, J. Power Sources 157 (2006) 217–221.
[120] X. Cui, J. Shi, H. Chen, L. Zhang, L. Guo, J. Gao, J. Li, J. Phys. Chem. B 112 (2008) 12024.
[121] J. Rajeswari, B. Viswanathan, T.K. Varadarajan, Mater. Chem. Phys. 106 (2007) 168–174.
[122] T. Maiyalagan, B. Viswanathan, J. Power Sources 175 (2008) 789–793.
[123] G.R. Patzke, F. Krumeich, R. Nesper, Angew. Chem. Int. Ed. 41 (2002) 2446–2461.
[124] S. Zhang, H. Zhu, H. Yu, J. Hou, B. Yi, P. Ming, Chin. J. Catal. 28 (2007) 109–111.
[125] M.K. Jeon, H. Daimon, K.R. Lee, A. Nakahara, S.I. Woo, Electrochem. Comm. 9 (2007) 2692–2695.
[126] H. Chhina, S. Campbell, O. Kesler, J. Power Sources 164 (2007) 431–440.
[127] H. Chhina, S. Campbell, O. Kesler, J. Power Sources 179 (2008) 50–59.
[128] Y. Hara, N. Minami, H. Itagaki, Appl. Catal. A 323 (2007) 86–93.
[129] Y. Hara, N. Minami, H. Matsumoto, H. Itagaki, Appl. Catal. A 332 (2007) 289–296.
[130] R. Ganesan, J.S. Lee, Angew. Chem. Int. Ed. 44 (2005) 6557–6560.
[131] Y. Wang, S. Song, V. Maragou, P.K. Shen, P. Tsiakaras, Appl. Catal. B 89 (2009) 223–228.
[132] R. Ganesan, D.J. Ham, J.S. Lee, Electrochem. Comm. 9 (2007) 2576–2579.
[133] D.J. Ham, Y.K. Kim, S.H. Han, J.S. Lee, Catal. Today 132 (2008) 117–122.
[134] Y. Wang, S. Song, P.K. Shen, C. Guo, C.M. Li, J. Mater. Chem. 19 (2009) 6149–6153.
[135] A. Micek-Ilnicka, J. Mol. Catal. A: Chem. 308 (2009) 1–14.
[136] U. Mioč, M. Davidovič, N. Tjapkin, Ph. Colomban, A. Novak, Solid State Ionics 46 (1991) 103–109.
[137] N. Giordano, P. Staiti, S. Hocevar, A.S. Aricò, Electrochim. Acta 41 (1996) 397–403.
[138] P. Staiti, S. Hocevar, N. Giordano, Int. J. Hydr. En. 22 (1997) 809–814.
[139] N. Giordano, P. Staiti, A.S. Aricò, E. Passalacqua, L. Abate, S. Hocevar, Electrochim. Acta 42 (1997) 1645–1652.
[140] P. Staiti, A.S. Aricò, V. Antonucci, S. Hocevar, J. Power Sources 70 (1998) 91–101.
[141] P. Staiti, S. Freni, S. Hocevar, J. Power Sources 79 (1999) 250–255.
[142] S.D. Mikhailenko, S. Kaliaguine, J.B. Moffat, Solid State Ionics 99 (1997) 281–286.
[143] Y.S. Kim, F. Wang, M. Hickner, T.A. Zawodzinski, J.E. McGrath, J. Membr. Sci. 212 (2003) 263–282.
[144] I. Colicchio, F. Wen, H. Keul, U. Simon, M. Moeller, J. Membr. Sci. 326 (2009) 45–57.
[145] Tatsumisago, S.Y. Honjo, Y. Sakai, T. Minami, Solid State Ionics 74 (1994) 105–108.
[146] D.R. Vernon, F. Meng, S.F. Dec, D.L. Williamson, J.A. Turner, A.M. Herring, J. Power Sources 139 (2005) 141–151.
[147] P. Staiti, A.S. Aricò, V. Baglio, F. Lufrano, E. Passalacqua, V. Antonucci, Solid State Ionics 145 (2001) 101–107.
[148] J.-D. Kim, T. Mori, I. Honma, J. Electrochem. Soc. 153 (2006) A508–A514.
[149] Z.-G. Shao, J. Prabhuram, I.-M. Hsing, J. Membr. Sci. 229 (2004) 43–51.
[150] V. Ramani, H.R. Kunz, J.M. Fenton, J. Membr. Sci. 279 (2006) 506–512.
[151] T. Fu, J. Wang, J. Ni, Z. Cui, S. Zhong, C. Zhao, H. Na, W. Xing, Solid State Ionics 179 (2008) 2265–2273.
[152] A.F. Ismail, N.H. Othman, A. Mustafa, J. Membr. Sci. 329 (2009) 18–29.
[153] I. Honma, S. Hirakawa, K. Yamada, J.M. Bae, Solid State Ionics 118 (1999) 29–36.
[154] I. Honma, Y. Takeda, J.M. Bae, Solid State Ionics 120 (1999) 255–264.

[155] I. Honma, S. Nomura, H. Nakajima, J. Membr. Sci. 185 (2001) 83–94.
[156] H. Nakajima, S. Nomura, T. Sugimoto, S. Nishikawa, I. Honma, J. Electrochem. Soc. 149 (2002) A953–A959.
[157] J.D. Kim, I. Honma, J. Electrochem. Soc. 151 (2004) A1396–1401.
[158] J.D. Kim, I. Honma, Electrochim. Acta 49 (2004) 3179–3183.
[159] J.D. Kim, I. Honma, Solid State Ionics 176 (2005) 547–552.
[160] V. Ramani, H.R. Kunz, J.M. Fenton, J. Membr. Sci. 232 (2004) 31–44.
[161] V. Ramani, H.R. Kunz, J.M. Fenton, Electrochim. Acta 50 (2005) 1181–1187.
[162] V. Ramani, H.R. Kunz, J.M. Fenton, J. Membr. Sci. 266 (2005) 110–114.
[163] V. Ramani, H.R. Kunz, J.M. Fenton, J. Power Sources 152 (2005) 182–188.
[164] Z. Cui, C. Liu, T. Lu, W. Xing, J. Power Sources 167 (2007) 94–99.
[165] M. Yamada, I. Honma, J. Phys. Chem. B 110 (2006) 20486–20490.
[166] A. Noda, M.A.B.H. Susan, K. Kudo, S. Mitsushima, K. Hayamizu, M. Watanabe, J. Phys. Chem. B 107 (2003) 4024–4033.
[167] J.-D. Kim, S. Hayashi, M. Onoda, A. Sato, C. Nishimura, T. Mori, I. Honma, Electrochim. Acta 53 (2008) 7638–7643.
[168] J.-D. Kim, S. Hayashi, T. Mori, I. Honma, Electrochim. Acta 53 (2007) 963–967.
[169] W.A. England, M.G. Cross, A. Hanmett, P.J. Wiseman, J.B. Goodenough, Solid State Ionics 1 (1980) 231–249.
[170] P. Barboux, R. Morineau, J. Uvage, Solid State Ionics 27 (1988) 221–225.
[171] Y.M. Li, M. Hibino, M. Miyayania, T. Kudo, Solid State Ionics 134 (2000) 271–279.
[172] Y. Tanaka, M. Miyayama, M. Hibino, T. Kudo, Solid State Ionics 171 (2004) 33–39.
[173] J. Yang, Y. Li, Y. Huang, J. Liang, P.K. Shen, J. Power Sources 177 (2008) 56–60.